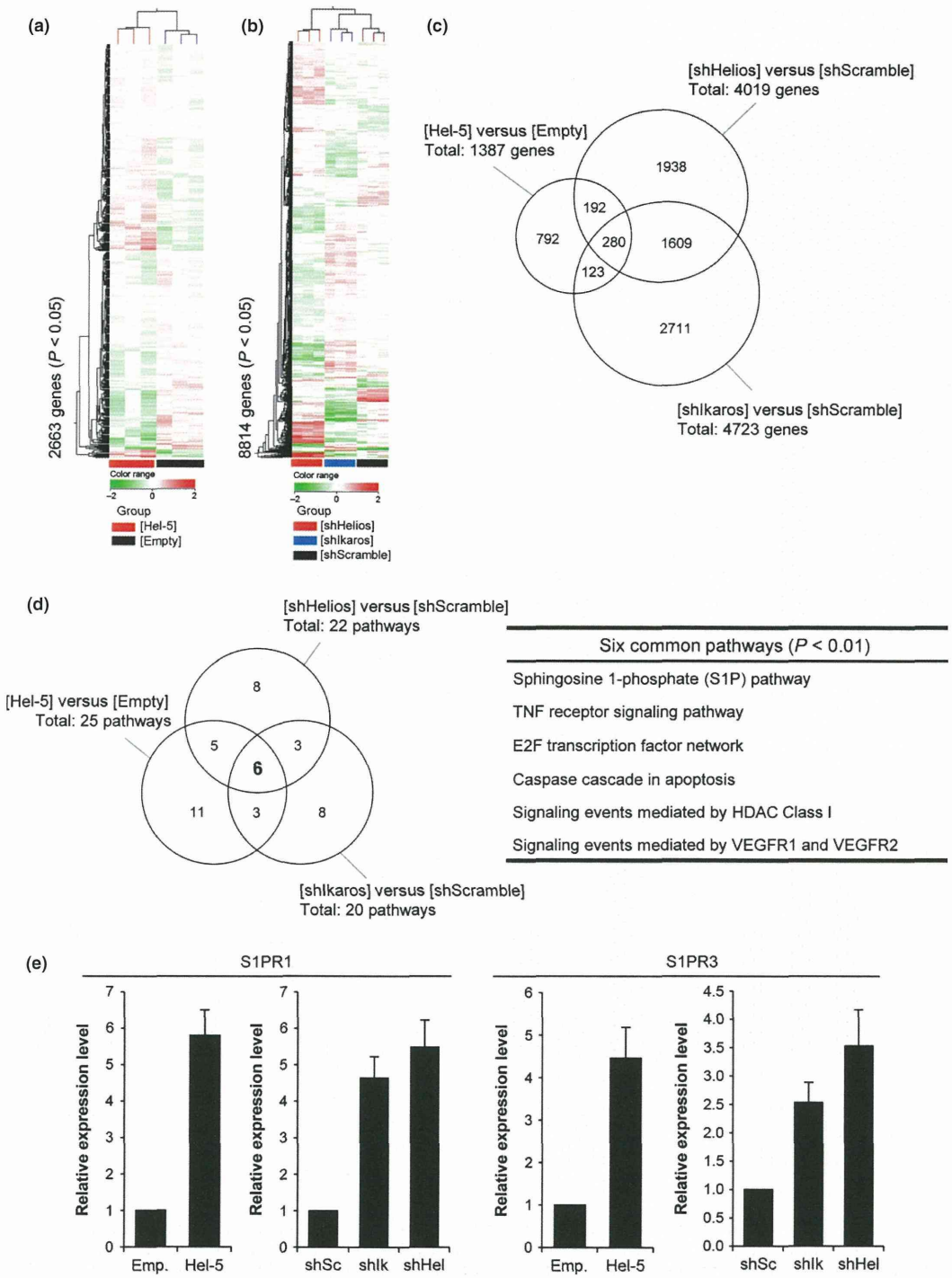

Fig. 7. Comprehensive search for Helios target genes by microarray analysis. (a,b) Gene expression analysis of Jurkat stable cells. The gene expression patterns of Jurkat cells expressing Hel-5 (n = 3), shIkaros (n = 3), and shHelios (n = 3) were comprehensively analyzed by microarray technique. The obtained 2D hierarchical clusters and Pearson's correlation between the cells expressing Hel-5 or not (a) and the cells introducing shHel, shIk, or shSc (b). (c) Venn diagram of differential gene expression pattern in the Jurkat sublines. The each differential expression gene set (5-fold changes, $P < 1 \times 10^{-5}$) was compared. (d) Venn diagram depicting the overlap between the outputs of pathway analysis in Jurkat sublines. The analysis was based on the NCI-Nature Pathway Interaction Database.[37] Each differential pathway set (t-test, $P < 0.01$) was compared and the common pathways listed. (e) Results of quantitative RT-PCR of shingosine-1-phosphate receptor 1 (S1PR1) and receptor 3 (S1PR3) in Jurkat sublines (n = 3, mean ± SD). HDAC, histone deacetylase; VEGFR, vascular endothelial growth factor receptor.

Acknowledgments

We thank Mr. M. Nakashima and Ms. T. Akashi for support and maintenance of the Joint Study on Prognostic Factors of ATL Development. This work is supported by JSPS KAKENHI Grant Numbers 24790436 (M.Y.), 23390250 (T.W.), 23659484 (T.W.), 23 6291 (S.A.), NEXT KAKENHI Grant Number 221S0001 (T.W.), and a Grant-in-Aid from the Ministry of Health, Labor and Welfare of Japan H24-G-004 (M.Y. and T.W.).

doi: 10.1111/cas.12181

Disclosure Statement

The authors have no conflict of interest.

References

1 Yamaguchi K, Watanabe T. Human T lymphotropic virus type-I and adult T-cell leukemia in Japan. *Int J Hematol* 2002; **76**: 240–45.
2 Iwanaga M, Watanabe T, Utsunomiya A *et al.* Human T-cell leukemia virus type I (HTLV-1) proviral load and disease progression in asymptomatic HTLV-1 carriers: a nationwide prospective study in Japan. *Blood* 2010; **116**: 1211–19.
3 Yamagishi M, Nakano K, Miyake A *et al.* Polycomb-mediated loss of miR-31 activates NIK-dependent NF-κB pathway in adult T cell leukemia and other cancers. *Cancer Cell* 2012; **21**: 121–35.
4 Yamagishi M, Watanabe T. Molecular hallmarks of adult T cell leukemia. *Front Microbiol* 2012; **3**: 334.
5 Lo K, Landau NR, Smale ST. LyF-1, a transcriptional regulator that interacts with a novel class of promoters for lymphocyte-specific genes. *Mol Cell Biol* 1991; **11**: 5229–43.
6 Georgopoulos K, Moore DD, Derfler B. Ikaros, an early lymphoid-specific-transcription factor and a putative mediator for T cell commitment. *Science* 1992; **258**: 808–12.
7 Hahm K, Ernst P, Lo K, Kim GS, Turck C, Smale ST. The lymphoid transcription factor LyF-1 is encoded by specific, alternatively spliced mRNAs derived from the Ikaros gene. *Mol Cell Biol* 1994; **14**: 7111–23.
8 Sun L, Liu A. Zinc finger-mediated protein interactions modulate Ikaros activity, a molecular control of lymphocyte development. *EMBO J* 1996; **15**: 5358–69.
9 Morgan B, Sun L, Avitahl N *et al.* Aiolos, a lymphoid restricted transcription factor that interacts with Ikaros to regulate lymphocyte differentiation. *EMBO J* 1997; **16**: 2004–13.
10 Kelley CM, Ikeda T, Koipally J *et al.* Helios, a novel dimerization partner of Ikaros expressed in the earliest hematopoietic progenitors. *Curr Biol* 1998; **8**: 508–15.
11 Cobb BS, McCarty AS, Brown KE *et al.* Helios, a T cell-restricted Ikaros family member that quantitatively associates with Ikaros at centromeric heterochromatin. *Genes Dev* 1998; **12**: 782–96.
12 Winandy S, Wu P, Georgopoulos K. A dominant mutation in the Ikaros gene leads to rapid development of leukemia and lymphoma. *Cell* 1995; **83**: 289–99.
13 Wang JH, Nichogiannopoulou A, Wu L *et al.* Selective defects in the development of the fetal and adult lymphoid system in mice with an Ikaros null mutation. *Immunity* 1996; **5**: 537–49.
14 Wang JH, Avitahl N, Cariappa A *et al.* Aiolos regulates B cell activation and maturation to effector state. *Immunity* 1998; **9**: 543–53.
15 Zhang Z, Swindle CS, Bates JT, Ko R, Cotta CV, Klug CA. Expression of a non-DNA-binding isoform of Helios induces T-cell lymphoma in mice. *Blood* 2007; **109**: 2190–7.
16 Sun L, Crotty ML, Sensel M *et al.* Expression of dominant-negative Ikaros isoforms in T-cell acute lymphoblastic leukemia. *Clin Cancer Res* 1999; **5**: 2112–20.
17 Nakase K, Ishimaru F, Avitahl N *et al.* Dominant negative isoform of the Ikaros gene in patients with adult B-cell acute lymphoblastic leukemia. *Cancer Res* 2000; **60**: 062–4065.
18 Takanashi M, Yagi T, Imamura T *et al.* Expression of the Ikaros gene family in childhood acute lymphoblastic leukaemia. *Br J Haematol* 2002; **117**: 525–30.
19 Nishii K, Katayama N, Miwa H. Non-DNA-binding Ikaros isoform gene expressed in adult B-precursor acute lymphoblastic leukemia. *Leukemia* 2002; **16**: 1285–92.
20 Tonnelle C, Imbert M-C, Sainty D, Granjeaud S, N'Guyen C, Chabannon C. Overexpression of dominant-negative Ikaros 6 protein is restricted to a subset of B common adult acute lymphoblastic leukemias that express high levels of the CD34 antigen. *Hematol J* 2003; **4**: 104–9.
21 Klein F, Feldhahn N, Herzog S *et al.* BCR-ABL1 induces aberrant splicing of IKAROS and lineage infidelity in pre-B lymphoblastic leukemia cells. *Oncogene* 2006; **25**: 1118–24.
22 Zhou F, Mei H, Jin R, Li X, Chen X. Expression of ikaros isoform 6 in chinese children with acute lymphoblastic leukemia. *J Pediatr Hematol Oncol* 2011; **33**: 429–32.
23 Mullighan CG, Miller CB, Radtke I *et al.* BCR-ABL1 lymphoblastic leukaemia is characterized by the deletion of Ikaros. *Nature* 2008; **453**: 110–14.
24 Kano G, Morimoto A, Takanashi M *et al.* Ikaros dominant negative isoform (Ik6) induces IL-3-independent survival of murine pro-B lymphocytes by activating JAK-STAT and up-regulating Bcl-xl levels. *Leuk Lymphoma* 2008; **49**: 965–73.
25 Iacobucci I, Lonetti A, Messa F *et al.* Expression of spliced oncogenic Ikaros isoforms in Philadelphia-positive acute lymphoblastic leukemia patients treated with tyrosine kinase inhibitors: implications for a new mechanism of resistance. *Blood* 2008; **112**: 3847–55.
26 Mullighan CG, Su X, Zhang J *et al.* Deletion of IKZF1 and prognosis in acute lymphoblastic leukemia. *N Engl J Med* 2009; **360**: 470–80.
27 Kuiper RP, Waanders E, van der Velden VHJ *et al.* IKZF1 deletions predict relapse in uniformly treated pediatric precursor B-ALL. *Leukemia* 2010; **24**: 1258–64.
28 Nakase K, Ishimaru F, Fujii K *et al.* Overexpression of novel short isoforms of Helios in a patient with T-cell acute lymphoblastic leukemia. *Exp Hematol* 2002; **30**: 313–17.
29 Fujii K, Ishimaru F, Tabayashi T *et al.* Over-expression of short isoforms of Helios in patients with adult T-cell leukaemia/lymphoma. *Br J Haematol* 2003; **120**: 986–9.
30 Fujiwara SI, Yamashita Y, Nakamura N *et al.* High-resolution analysis of chromosome copy number alterations in angioimmunoblastic T-cell lymphoma and peripheral T-cell lymphoma, unspecified, with single nucleotide polymorphism-typing microarrays. *Leukemia* 2008; **22**: 1891–8.
31 Fujimoto R, Ozawa T, Itoyama T, Sadamori N, Kurosawa N, Isobe M. HELIOS-BCL11B fusion gene involvement in a t(2;14)(q34;q32) in an adult T-cell leukemia patient. *Cancer Genet* 2012; **205**: 356–64.
32 Shimoyama M. Diagnostic criteria and classification of clinical subtypes of adult T-cell leukaemia-lymphoma. A report from the Lymphoma Study Group (1984–87). *Br J Haematol* 1991; **79**: 428–37.
33 Tabayashi T, Ishimaru F, Takata M *et al.* Characterization of the short isoform of Helios overexpressed in patients with T-cell malignancies. *Cancer Sci* 2007; **98**: 182–8.
34 Kathrein KL, Chari S, Winandy S. Ikaros directly represses the notch target gene Hes1 in a leukemia T cell line: implications for CD4 regulation. *J Biol Chem* 2008; **283**: 10476–84.
35 Kleinmann E, Geimer Le Lay AS, Sellars M, Kastner P, Chan S. Ikaros represses the transcriptional response to Notch signaling in T-cell development. *Mol Cell Biol* 2008; **28**: 7465–75.
36 Molnár A, Georgopoulos K. The Ikaros gene encodes a family of functionally diverse zinc finger DNA-binding proteins. *Mol Cell Biol* 1994; **14**: 8292–303.
37 Schaefer CF, Anthony K, Krupa S *et al.* PID: the pathway interaction database. *Nucleic Acids Res* 2009; **37**: D674–9.
38 Pancewicz J, Taylor JM, Datta A. Notch signaling contributes to proliferation and tumor formation of human T-cell leukemia virus type 1-associated adult T-cell leukemia. *Proc Natl Acad Sci USA* 2010; **107**: 16619–24.
39 Murata K, Hattori M, Hirai N *et al.* Hes1 directly controls cell proliferation through the transcriptional repression of p27Kip1. *Mol Cell Biol* 2005; **25**: 4262–71.
40 Maeda Y, Seki N, Sato N, Sugahara K, Chiba K. Sphingosine 1-phosphate receptor type 1 regulates egress of mature T cells from mouse bone marrow. *Int Immunol* 2010; **22**: 515–25.
41 Spiegel S, Milstien S. The outs and the ins of sphingosine-1-phosphate in immunity. *Nat Rev Immunol* 2011; **11**: 403–15.
42 Maceyka M, Harikumar KB, Milstien S, Spiegel S. Sphingosine-1-phosphate signaling and its role in disease. *Trends Cell Biol* 2012; **22**: 50–60.
43 Ghigna C, Valacca C, Biamonti G. Alternative splicing and tumor progression. *Curr Genomics* 2008; **9**: 556–70.
44 David CJ, Manley JL. Alternative pre-mRNA splicing regulation in cancer: pathways and programs unhinged. *Genes Dev* 2010; **24**: 2343–64.
45 Blair CA, Zi X. Potential molecular targeting of splice variants for cancer treatment. *Indian J Exp Biol* 2011; **49**: 836–9.

Supporting Information

Additional Supporting Information may be found in the online version of this article:

Fig. S1. Deregulated expression of Ikaros family genes in primary adult T-cell leukemia cells.

Fig. S2. Colocalization of wild-type Ikaros and adult T-cell leukemia-type Helios.

Fig. S3. Dominant-negative inhibition of Hel-6, Hel-v1, and Hel-v2 in the suppressive activities of wild-type Helios and Ikaros.

Fig. S4. Downregulation of the expression of Helios mRNA in HTLV-1-positive T cell lines.

Fig. S5. Overexpression of abnormal Helios isoforms lacking exon 6 in adult T-cell leukemia samples.

Fig. S6. Relative value of Helios transcripts skipping exon 3 to all is upregulated in primary adult T-cell leukemia cells.

Fig. S7. Upregulated expression of Hes1 in primary adult T-cell leukemia cells.

Table S1. Clinical characteristics of adult T-cell leukemia patients and HTLV-1 carriers.

Table S2. Primer list and probe sequences.

doi: 10.1111/cas.12181

OPEN ACCESS Freely available online

PLOS ONE

The CD3 versus CD7 Plot in Multicolor Flow Cytometry Reflects Progression of Disease Stage in Patients Infected with HTLV-I

Seiichiro Kobayashi[1], Yamin Tian[1,2], Nobuhiro Ohno[3], Koichiro Yuji[3], Tomohiro Ishigaki[4], Masamichi Isobe[3], Mayuko Tsuda[3], Naoki Oyaizu[5], Eri Watanabe[4], Nobukazu Watanabe[4], Kenzaburo Tani[2], Arinobu Tojo[1,3], Kaoru Uchimaru[3]*

1 Division of Molecular Therapy, Institute of Medical Science, The University of Tokyo, Tokyo, Japan, **2** Department of Molecular Genetics, Medical Institute of Bioregulation, Kyushu University, Fukuoka, Japan, **3** Department of Hematology/Oncology, Research Hospital, Institute of Medical Science, The University of Tokyo, Tokyo, Japan, **4** Laboratory of Diagnostic Medicine, Division of Stem Cell Therapy, Institute of Medical Science, The University of Tokyo, Tokyo, Japan, **5** Clinical Laboratory, Research Hospital, Institute of Medical Science, The University of Tokyo, Tokyo, Japan

Abstract

Purpose: In a recent study to purify adult T-cell leukemia-lymphoma (ATL) cells from acute-type patients by flow cytometry, three subpopulations were observed in a CD3 versus CD7 plot (H: $CD3^{high}CD7^{high}$; D: $CD3^{dim}CD7^{dim}$; L: $CD3^{dim}CD7^{low}$). The majority of leukemia cells were enriched in the L subpopulation and the same clone was included in the D and L subpopulations, suggesting clonal evolution. In this study, we analyzed patients with indolent-type ATL and human T-cell leukemia virus type I (HTLV-I) asymptomatic carriers (ACs) to see whether the CD3 versus CD7 profile reflected progression in the properties of HTLV-I-infected cells.

Experimental Design: Using peripheral blood mononuclear cells from patient samples, we performed multi-color flow cytometry. Cells that underwent fluorescence-activated cell sorting were subjected to molecular analyses, including inverse long PCR.

Results: In the D(%) versus L(%) plot, patient data could largely be categorized into three groups (Group 1: AC; Group 2: smoldering- and chronic-type ATL; and Group 3: acute-type ATL). Some exceptions, however, were noted (*e.g.*, ACs in Group 2). In the follow-up of some patients, clinical disease progression correlated well with the CD3 versus CD7 profile. In clonality analysis, we clearly detected a major clone in the D and L subpopulations in ATL cases and, intriguingly, in some ACs in Group 2.

Conclusion: We propose that the CD3 versus CD7 plot reflects progression of disease stage in patients infected with HTLV-I. The CD3 versus CD7 profile will be a new indicator, along with high proviral load, for HTLV-I ACs in forecasting disease progression.

Citation: Kobayashi S, Tian Y, Ohno N, Yuji K, Ishigaki T, et al. (2013) The CD3 versus CD7 Plot in Multicolor Flow Cytometry Reflects Progression of Disease Stage in Patients Infected with HTLV-I. PLoS ONE 8(1): e53728. doi:10.1371/journal.pone.0053728

Editor: Jean-Pierre Vartanian, Institut Pasteur, France

Received August 31, 2012; **Accepted** December 4, 2012; **Published** January 22, 2013

Funding: This study was supported by the Ministry of Education, Culture, Sports, Science and Technology, Japan. The funders had no role in study design, data collection and analysis, decision to publish, or preparation of the manuscript.

Competing Interests: The authors have declared that no competing interests exist.

* E-mail: uchimaru@ims.u-tokyo.ac.jp

Introduction

Human T-cell leukemia virus type I (HTLV-I) is the agent that causes HTLV-I-associated diseases, such as adult T-cell leukemia-lymphoma (ATL), HTLV-I-associated myelopathy/tropical spastic paraparesis (HAM/TSP), and HTLV-I uveitis (HU) [1–3]. Approximately 10–20 million people are infected with the HTLV-I virus worldwide [4]. The lifetime risk of developing ATL is estimated to be approximately 2.5–5% [5,6]. ATL includes a spectrum of diseases that are referred to as smoldering-, chronic-, lymphoma-, and acute-type [7,8]. The chronic and smoldering types of ATL are considered indolent and are usually managed with watchful waiting until the disease progresses to aggressive (lymphoma- or acute-type) ATL [9]. Because the prognosis of ATL is poor with current treatment strategies, factors to forecast progression to ATL from asymptomatic carriers (ACs) have been researched [10–13] in the hope that they will be useful for preventive therapy under development in the early malignant stage.

Various cellular dysfunctions induced by viral genes (*e.g.*, tax and HBZ), genetic and epigenetic alterations, and the host immune system are considered to cooperatively contribute to leukemogenesis in ATL [14–16]. However, the complex mechanism may hinder determination of a clear mechanism of the pathology and make discovery of risk factors difficult. In a prospective nationwide study in Japan, high proviral load (VL,

Table 1. Clinical profile of patients infected with HTLV-I and normal controls.

Clinical sutype	Number of cases	Male	Female	Age (range)	WBC(/μl) (range)	Lymphocytes(%) (range)	Abnormal lymphocytes(%) (range)
HTLV-1 AC	40	12	28	49.9 (28–70)	5525 (2680–10360)	35.9 (22.4–59.5)	0.9 (0.0–4.4)
Smoldering	7	4	3	55.3 (43–77)	5944 (3680–8710)	32.5 (13.4–47.5)	5.8 (0.7–16.5)
Chronic	7	4	3	52.7 (37–60)	9180 (4070–12790)	45.8 (35.0–61.5)	9.2 (3.4–12.7)
Acute	13	4	9	58.8 (42–74)	15328 (4450–41480)	16.3 (1.7–50.5)	40.3 (3.0–89.6)
Normal controls	10	6	4	47.4 (27–66)	ND	ND	ND

WBC: white blood cells (normal range, 3500–9100/μl).
AC: asymptomatic carrier.
ND: analysis were not performed.
Average of age, WBC, lymphocytes (%) and abnormal lymphocytes (%) are shown.
The proportion of abonormal lymphocytes in peripheral blood WBCs was evaluated by morphological exmanination.
doi:10.1371/journal.pone.0053728.t001

over 4.17 copies/100 peripheral blood mononuclear cells) was found to be a major risk factor for HTLV-I AC developing into ATL [13]. Although VL indicates the proportion of HTLV-I-infected cells, it does not indicate size or degree of malignant progression in each clone; *i.e.*, it does not directly indicate progression of disease stage in HTLV-I infection. Moreover, the majority of ACs with high VL remained intact during the study period, indicating that a more accurate indicator of progression is needed.

In our recent study to purify monoclonal ATL cells from acute-type patients by flow cytometry, three subpopulations were observed in a CD3 versus CD7 plot of $CD4^+$ cells (H: $CD3^{high}CD7^{high}$, D: $CD3^{dim}CD7^{dim}$, L: $CD3^{dim}CD7^{low}$), and the majority of ATL cells were enriched in the L subpopulation [17]. Clonality analyses revealed that the D and L subpopulations contained the same clone, suggesting clonal evolution of HTLV-I-infected cells to ATL cells. From these findings, we speculated that the CD3 versus CD7 profile may reflect disease progression in HTLV-I infection. In this study, the CD3 versus CD7 profile by flow cytometry, combined with molecular (clonality and proviral load) characterizations, were analyzed in patients with various clinical subtypes (HTLV-I AC, and indolent and aggressive ATL). We found that the CD3 versus CD7 profile reflected disease progression of HTLV-I-infected cells to ATL cells. We also discuss the significance of this analysis as a novel risk indicator for HTLV-I ACs in forecasting progression to ATL.

Materials and Methods

Cell lines and patient samples

TL-Om1, an HTLV-I-infected cell line, established Dr. Hinuma's laboratory [18], was provided by Dr. Toshiki Watanabe (The University of Tokyo, Tokyo, Japan) and was cultured in RPMI-1640 medium containing 10% fetal bovine serum. Peripheral blood samples were collected from inpatients and outpatients at our hospital from August 2009 to November 2011. All patients with ATL were categorized according to Shimoyama's criteria [7,8]. Patients with various complications, such as autoimmune disorder and systemic infections, were excluded. Lymphoma-type patients were excluded because ATL cells are not considered to exist in peripheral blood of this clinical subtype. In patients with ATL receiving chemotherapy, blood samples were collected before treatment or during the recovery phase between chemotherapy sessions. Samples collected from 10 healthy volunteers (mean age: 47.4 years; range: 27–66 years) were used as normal controls.

The present study was approved by the research ethics committee of the institute of medical science, the university of Tokyo. Subjects provided written informed consent.

Flow cytometry and cell sorting

Peripheral blood mononuclear cells (PBMCs) were isolated from heparin-treated whole blood by density gradient centrifugation, as described previously [17]. Cells were stained using a combination of phycoerythrin (PE)-CD7, APC-Cy7-CD3, Pacific Blue-CD4, and Pacific Orange-CD14. Pacific Orange-CD14 was purchased from Caltag-Invitrogen (Carlsbad, CA). All other antibodies were obtained from BD BioSciences (San Jose, CA). Propidium iodide (PI; Sigma, St. Louis, MO) was added to the samples to stain dead cells immediately prior to flow cytometry. A BD FACS Aria instrument (BD Immunocytometry Systems, San Jose, CA) was used for all multicolor flow cytometry and cell sorting. Data were analyzed using the FlowJo software (Treestar, San Carlos, CA).

Quantification of HTLV-I proviral load by real-time quantitative polymerase chain reaction (PCR)

The HTLV-I proviral load in FACS-sorted PBMCs was quantified by real-time quantitative polymerase chain reaction (PCR; TaqMan method) using the ABI Prism 7000 sequence detection system (Applied Biosystems, Foster City, CA) as described previously [13,17]. Briefly, 50 ng of genomic DNA was extracted from human PBMCs using a QIAamp DNA blood Micro kit (Qiagen, Hilden, Germany). Triplicate samples of the DNA were amplified. Each PCR mixture, containing an HTLV-I pX region-specific primer pair at 0.1 μM (forward primer 5′-CGGATACCCAGTCTACGTGTT-3′ and reverse primer 5′-

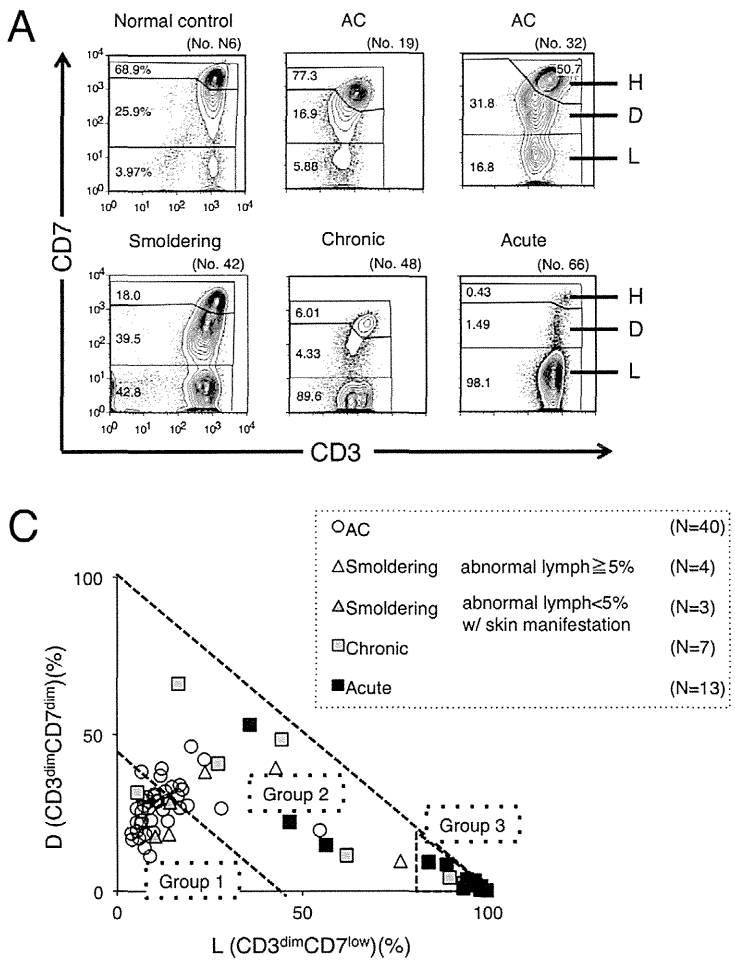

Figure 1. CD3 versus CD7 plots in flow cytometric analysis of patients who are asymptomatic HTLV-I carriers (ACs) and have various clinical subtypes of adult T-cell leukemia-lymphoma (ATL) suggest disease progression in HTLV-I infection. (A) Flow cytometric profile of an AC, various clinical subtypes of ATL (smoldering, chronic, and acute), and a normal control. Representative cases of CD3 versus CD7 plots in $CD4^+$ cells are shown. (B) A two-dimensional plot of AC cases showing the percentage of the D and L subpopulations by flow cytometry. AC cases were divided into two groups according to HTLV-I VL (greater or less than 4%). The border line (45% of D+L subpopulations) between Group 1 and 2 was set based on proviral load (VL). All AC cases with less than 4% VL were included in Group 1. All AC cases included in Group 2 had greater than 4% VL. VL<4%: n = 21; VL>4%: n = 19. All VL data in this figure were provided from the database of the Joint Study on Predisposing Factors of ATL Development (JSPFAD). (C) A two-dimensional plot of all patients showing the percentage of the D and L subpopulations. The smoldering type was divided into two categories: smoldering type with greater than 5% abnormal lymphocytes and smoldering type with less than 5% abnormal lymphocytes with skin manifestation. The two diagonal dotted lines indicate 45% and 100% of D+L subpopulations (*i.e.*, 55% and 0% of the H subpopulation). Data were categorized into three groups.
doi:10.1371/journal.pone.0053728.g001

CAGTAGGGCGTGACGATGTA-3′), FAM-labeled probe at 0.1 μM (5′- CTGTGTACAAGGCGACTGGTGCC-3′), and 1× TaqMan Universal PCR master mix (Applied Biosystems), was subjected to 50 cycles of denaturation (95°C, 15 seconds) and annealing to extension (60°C, 1 minute), following an initial Taq polymerase activation step (95°C, 10 minutes). The RNase P control reagent (Applied Biosystems) was used as an internal control for calculating the input cell number (using VIC reporter dye). DNAs extracted from TL-Om1 and normal human PBMCs were used as positive and negative controls, respectively. The HTLV-I proviral load (%) was calculated as the copy number of the pX region per input cell number. To correct the deviation of data acquired in each experiment, data from TL-Om1 (positive control) were adjusted to 100%, and the sample data were corrected accordingly by a proportional calculation.

Inverse long PCR

For clonality analysis, inverse long PCR was performed [17]. First, 1 μg of genomic DNA extracted from the FACS-sorted cells was digested with *Eco*RI and *Pst*I at 37°C overnight. Purification of DNA fragments was performed using a QIAEX2 gel extraction kit (Qiagen). The purified DNA was self-ligated with T4 DNA ligase (Takara Bio, Otsu, Japan) at 16°C overnight. The circular DNA obtained from the *Eco*RI digestion fragment was then digested

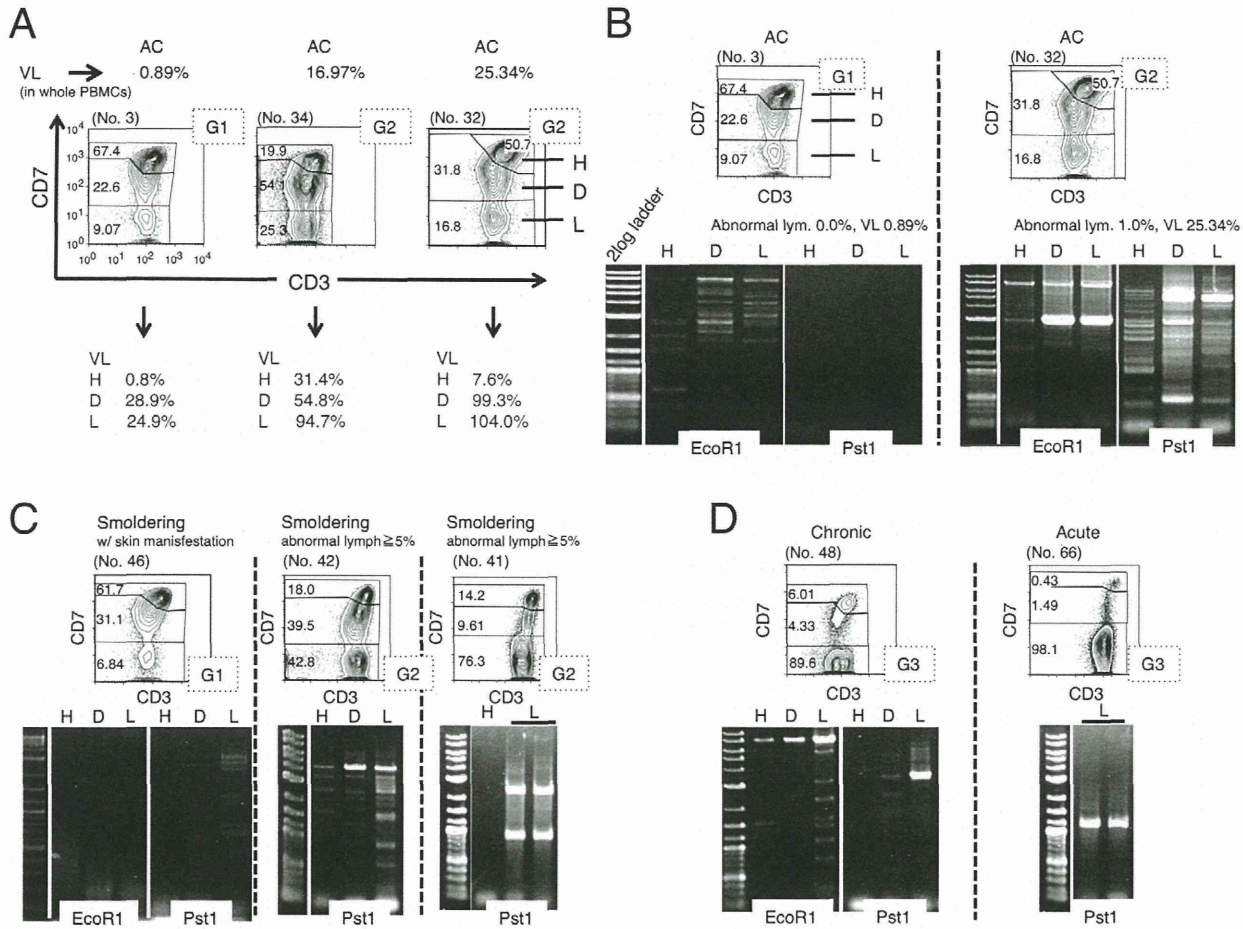

Figure 2. HTLV-I proviral load (VL) and clonality in each subpopulation, based on the CD3 versus CD7 plot. (A) The three subpopulations (H, D, L) based on the CD3 versus CD7 plot were subjected to fluorescence-activated cell sorting (FACS) and VL analysis. Three representative cases are shown. G1 or G2 in the dotted box indicates Group 1 or Group 2, categorized by the percentage of the D and L subpopulations, respectively. (B)–(D) Analysis of clonality in the three subpopulations based on the CD3 versus CD7 plot. Genomic DNA was extracted from FACS-sorted cells of each subpopulation and subjected to inverse long polymerase chain reaction (PCR). Representative data of two cases of AC (B), three cases of smoldering type, including one with skin manifestations (C), and cases of a chronic type and an acute type (D) are shown. PCR was performed in duplicate (black bars) in cases when a sufficient amount of DNA was obtained.
doi:10.1371/journal.pone.0053728.g002

with *Mlu*I, which cuts the pX region of the HTLV-I genome and prevents amplification of the viral genome. Inverse long PCR was performed using Takara LA *Taq* polymerase (Takara Bio). For the *Eco*RI-treated template, the forward primer was 5′-TGCCTGACCCTGCTTGCTCAACTCTACGTCTTTG-3′ and the reverse primer was 5′-AGTCTGGGCCCT-GACCTTTTCAGACTTCTGTTTC-3′. For the *Pst*I-treated group, the forward primer was 5′-CAGCCCATTCTATAG-CACTCTCCAGGAGAG-3′ and the reverse primer was 5′-CAGTCTCCAAACACGTAGACTGGGTATCCG-3. Each 50-μL reaction mixture contained 0.4 mM of each dNTP, 25 mM $MgCl_2$, 10× LA PCR buffer II containing 20 mM Tris-HCl and 100 mM KCl, 0.5 mM of each primer, 2.5 U LA *Taq* polymerase, and 50 ng of the processed genomic DNA. The reaction mixture was subjected to 35 cycles of denaturation (94°C, 30 seconds) and annealing to extension (68°C, 8 minutes). Following PCR, the products were subjected to electrophoresis on 0.8% agarose gels. In samples from which a sufficient amount of DNA was extracted, PCRs were performed in duplicate.

Results

CD3 versus CD7 profile in flow cytometry in various clinical subtypes of patients infected with HTLV-I

The clinical profiles of the 77 cases analyzed in this study are shown in Table 1. According to the gating procedure, as shown in Figure S1 [17], we constructed a CD3 versus CD7 plot of $CD4^+$ cells in PBMCs of various clinical subtypes from patients infected with HTLV-I and normal controls. The three subpopulations ($CD3^{high}CD7^{high}$, $CD3^{dim}CD7^{dim}$, and $CD3^{dim}CD7^{low}$) observed are referred to as the H, D, and L subpopulations, respectively. Representative results for each clinical subtype of HTLV-I infection are shown in Figure 1A. Regarding the data for an acute-type patient (no. 66), the dominant population was the L subpopulation, in which we previously demonstrated that monoclonal ATL cells are enriched [17]. Regarding the AC (no. 19), the CD3 versus CD7 profile was close to that of the normal control, although in some AC cases, such as no. 32, the profile differed from that of the normal control, because in contrast to case no. 19,

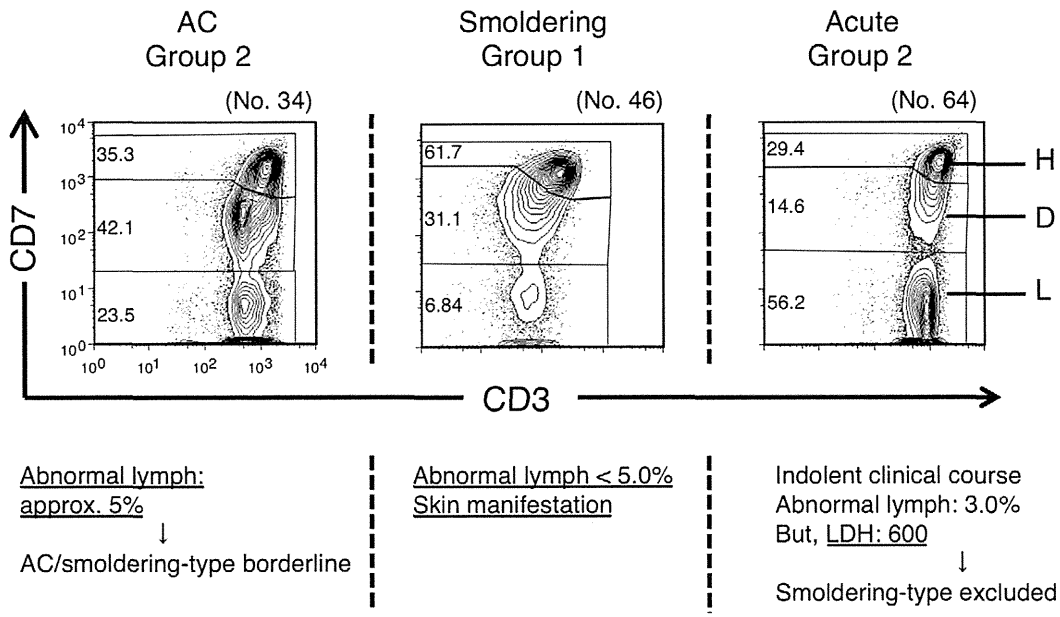

Figure 3. Study of exceptional cases categorized by proportion of the $CD3^{dim}CD7^{dim}$ (D) and $CD3^{dim}CD7^{low}$ (L) subpopulations. Left: An HTLV-I AC patient who was categorized in Group 2 in the D(%) versus L(%) plot. Middle: A patient with smoldering-type ATL who was categorized in Group 1. Right: A patient with acute-type ATL who was categorized in Group 2.
doi:10.1371/journal.pone.0053728.g003

these cases had increased D and L subpopulations. Regarding the data for indolent-type disease (smoldering and chronic), increases in the D and L subpopulations were intermediate between ACs and patients with acute-type disease. These representative flow cytometric data suggest that continuity in the CD3 versus CD7 profile seemed to exist among the various clinical subtypes of patients infected with HTLV-I.

The proportions of D and L subpopulations in all AC cases analyzed are shown in Figure 1B. Because the high HTLV-I proviral load (VL) in whole PBMCs, a VL of >4%, was reported to be a major risk indicator for progression to ATL [13], a border line was set based on VL. Group 1, the area under the diagonal line (D+L = 45%), included all AC cases with VLs of <4%. ACs with VLs of >4% were distributed between Groups 1 and 2. The proportions of D and L subpopulations in normal controls are shown in Figure S2. In this plot, all data for normal controls were distributed in Group 1. Data for all clinical subtypes are shown in Figure 1C. Most data for acute-type patients were located in the area beyond 80% of the L subpopulation and we designated this area as Group 3. Group 2, which is located between Group 1 and Group 3, included the majority of indolent-type (smoldering and chronic) cases. From these results, the three groups in the D(%) versus L(%) plot seemed to represent disease stage in each case.

Proviral load and clonality in each subpopulation in the CD3 versus CD7 plot

To further characterize each subpopulation (H, D, and L) in the CD3 versus CD7 plot, cells in each subpopulation were FACS-sorted and subjected to analysis of VL to determine the percentage of HTLV-I-infected cells in each subpopulation. Results for representative cases are shown in Figure 2A. The VL in whole PBMCs of an AC (no. 3) was low (0.89%). As expected, the VL in H, the major subpopulation, was low (0.8%). However, VLs in the D and L subpopulations were considerably higher (28.9% and 24.9%, respectively), indicating that HTLV-I-infected cells are relatively concentrated in these subpopulations. In the cases with high VLs in whole PBMCs (no. 32 with 25.34%; no. 34 with 16.97%), the VLs were also higher in the D and L subpopulations, and almost all cells in the L subpopulation were HTLV-I-infected.

In HTLV-I infection, progression to ATL requires several pathological steps, including clonal expansion [15]. To further characterize the three subpopulations based on the CD3 versus CD7 plot, we analyzed clonality in each subpopulation in patients with various clinical subtypes using the inverse long PCR method. Figure 2B shows two cases of AC. In the left case (no. 3), included in Group 1 in the D(%) and L(%) plot, multiple bands suggestive of multiple small clones were detected in the three subpopulations. However, no major band suggestive of a dominant clone was observed. In the right case (no. 32), included in Group 2, inverse long PCR of the FACS-sorted subpopulations suggested that the D and L subpopulations contained a major clone (Figure 2B). The D subpopulation had bands of the same size as those of the L subpopulation, indicating that the two distinct subpopulations contained a common major clone. Eleven cases of AC were included in Group 2. All three cases analyzed by Southern blotting (whole blood samples) were positive for clonal bands (Figure S3). In Figure 2C, data for three smoldering cases are shown. In case no. 46 (left), whose only manifestation was a skin eruption with few abnormal lymphocytes (less than 5% of white blood cells) in the peripheral blood, only faint minor bands suggestive of small clones were observed. In contrast, in the other two cases (nos. 42 and 41), intense bands suggestive of major clones were observed in both the D and L subpopulations. In no. 41 (right), weak bands were not visible, which suggested the selection of dominant clones. In Figure 2D, data for a chronic-type case and an acute-type case are shown. In both cases, intense bands in the L subpopulation suggest the existence of a major clone. The series of clonality analyses indicated that a major clone became more evident and the clinical

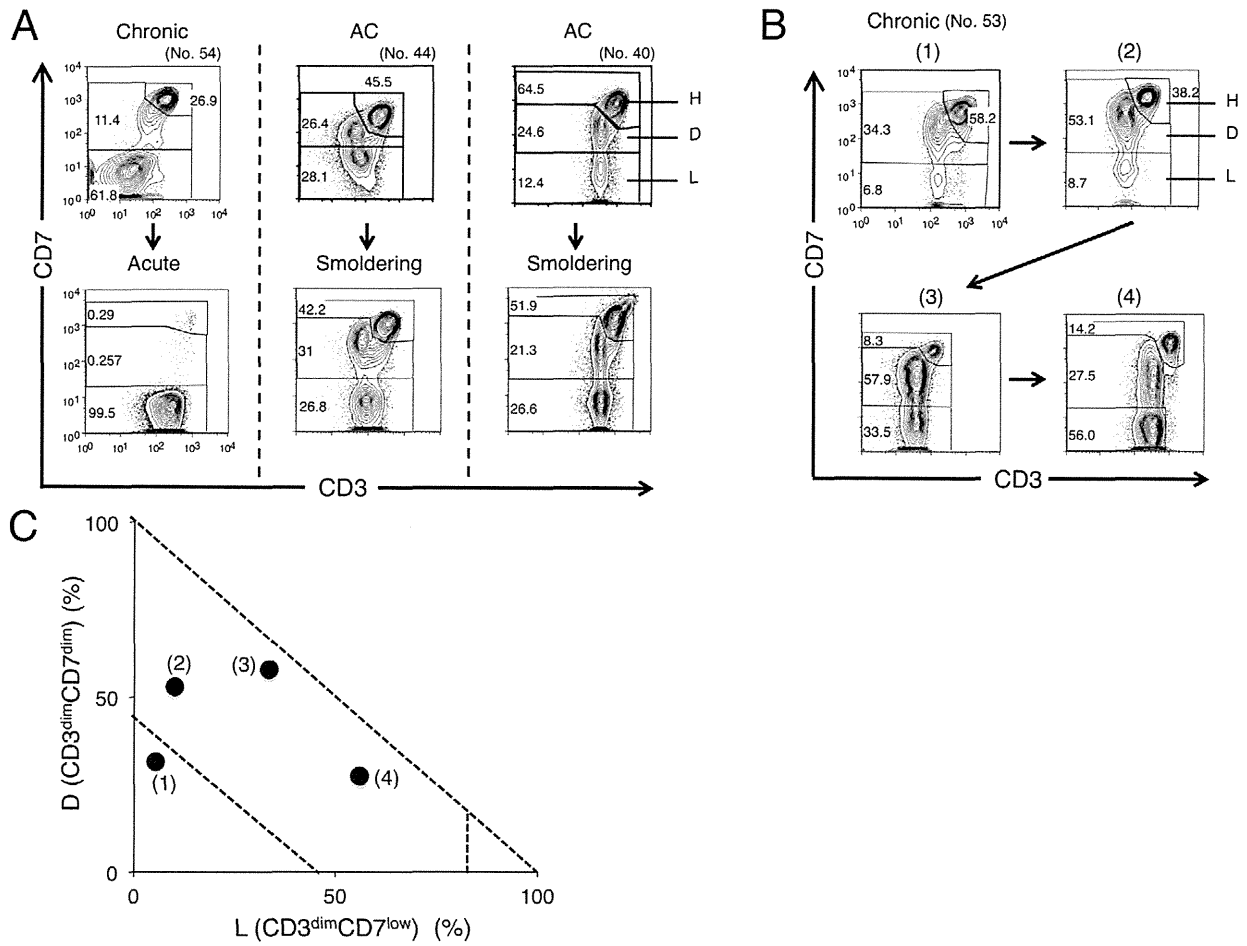

Figure 4. Alteration in the CD3 versus CD7 profile by flow cytometry in accordance with disease progression. (A) Change in the CD3 versus CD7 profile in representative cases. In all three cases shown, change in clinical data (*e.g.*, abnormal lymphocyte, LDH) resulted in progression of the clinical subtype. (B) Change in the CD3 versus CD7 profile in a time course in the case of chronic-type ATL. Clinical data are shown in Table S1. (C) Flow cytometric data in (B) are summarized in the D(%) versus L(%) plot.
doi:10.1371/journal.pone.0053728.g004

stage became more advanced as the D and L subpopulations increased.

Clinical evaluation of exceptional cases categorized by proportions of the $CD3^{dim}CD7^{dim}$ (D) and $CD3^{dim}CD7^{low}$ (L) subpopulations

As noted above, the D(%) versus L(%) plot generally represented disease stage in HTLV-I infection. However, we observed one case of chronic-type disease and three cases of smoldering-type disease in Group 1 and three cases of acute-type disease in Group 2. Furthermore, some ACs with VLs of >4% were observed in Group 2. Representative data from these apparently exceptional cases are shown in Figure 3. On the left, a case of AC (no. 34) observed in Group 2 is shown. 4.7% of lymphocytes in this blood sample were abnormal and clonality analysis by Southern blotting showed oligoclonal bands suggestive of clones of substantial size (Figure S3). These clinical data suggest that the disease stage would be around the AC/smoldering borderline. In the middle, a case of a smoldering type (no. 46) observed in Group 1 is shown. In this case, the percentage of abnormal lymphocytes in the peripheral blood was only 1%, but she had a histologically proven ATL lesion in the skin and was diagnosed with smoldering-type ATL. The other two smoldering cases categorized in Group 1 were the same as this case. These results indicate that ATL cells in these three smoldering cases infiltrated the skin, but not the peripheral blood. On the right, a case of acute-type disease categorized as Group 2 (no. 64) is shown. The clinical course of this patient was relatively indolent compared with typical acute-type disease. He had skin infiltration of ATL cells, but no lymph node swelling. However, LDH exceeded 1.5 times the upper limit of the normal range, which excludes a diagnosis of smoldering-type disease. Other acute-type cases categorized in Group 2 were diagnosed as such according to Shimoyama's criteria, but also had the same indolent clinical course as case no. 64. These cases should have been regarded as indolent ATL.

Changes in the CD3 versus CD7 profile in flow cytometry with disease progression

In several cases, we could obtain time-sequential samples (Figure 4). The patient (no. 54) shown on the left in Figure 4A progressed from chronic-type to acute-type disease. In flow cytometric analysis, decreases in the H and D subpopulations

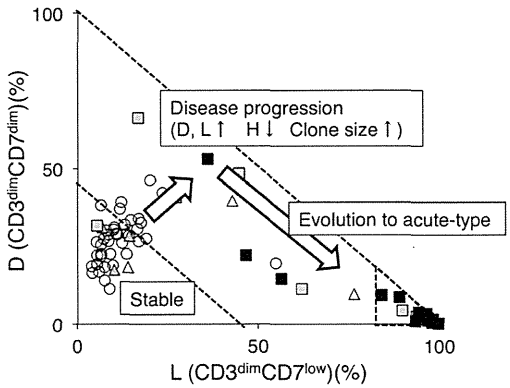

Figure 5. Summary of the study: the CD3 versus CD7 profile reflects progression of disease stage in patients infected with HTLV-I. In the percentage of D ($CD3^{dim}CD7^{dim}$) versus L ($CD3^{dim}CD7^{low}$) plot, Group 1 includes the majority of AC cases. As disease stage progresses, the CD3 versus CD7 profile then changes. With downregulation of CD3 and CD7, the D and L subpopulations increase gradually (Group 2). During this step, clones in the D and L subpopulations increase in size. Further accumulation of genetic alterations will result in rapid expansion of ATL clones—*i.e.*, evolution to acute-type ATL. In this step, the CD3 versus CD7 profile will progress from Group 2 to 3.
doi:10.1371/journal.pone.0053728.g005

and an increase in the L subpopulation were observed, indicating that disease progression correlated well with the change in the CD3 versus CD7 profile. The patients in the middle (no. 44) and on the right (no. 40) were included in Group 2 at the AC stage and later progressed to smoldering-type ATL. Although variation in the change of the flow cytometric profile was seen between these patients, the results suggest that ACs in Group 2 are at high risk of developing ATL.

The patient in Figure 4B (no. 53) was initially diagnosed with AC and later progressed to chronic-type ATL. Although the initial clinical course was stable, an increase in abnormal lymphocyte numbers was later observed, and low-dose VP-16 therapy (50 mg/day) was initiated because of hypoxemia due to lung infiltration of ATL cells. Table S1 and Figure 4C show summaries of the clinical data and the flow cytometric analyses, respectively. The flow cytometric data correlated well with disease progression.

Discussion

Findings in our previous analysis of acute-type ATL samples prompted our analysis of various clinical subtypes of patients infected with HTLV-I to examine whether the CD3 versus CD7 profile reflects the progression of oncogenesis in HTLV-I-infected cells [17]. Representative flow cytometric data shown in Figure 1A suggested that the CD3 versus CD7 profile changed during disease progression. As the disease stage progressed, the D and L subpopulations increased with concomitant decreases in the $CD3^{high}CD7^{high}$(H) subpopulation. Figure 1C, a summary of the flow cytometric data of all cases analyzed, reveals that the two-dimensional plot of the proportions of the D versus L subpopulations could divide all cases into three groups. Group 1, the area under the diagonal line, equivalent to 55% of the H subpopulation in which all normal controls were included (Figure S2), contained the majority of HTLV-I ACs. Group 3 was the area beyond 80% of the L subpopulation, and the majority of acute-type cases were included in this group. Group 2, located between Groups 1 and 3 (*i.e.*, less than 55% of the H subpopulation and 80% of the L subpopulation), included indolent-type (smoldering and chronic) cases and some AC cases. These results suggest that the CD3 versus CD7 expression profile reflects disease stage. Initially, both the D and L subpopulations gradually and simultaneously increased. However, at the clinically advanced stage, the increase in the L subpopulation was prominent. The change is considered to reflect the biological difference between the D and L subpopulations, which needs to be clarified.

In HTLV-I infection, the small clones of infected cells are considered to coexist from the AC stage [19,20]. A selected clone from the multiple small clones then grows and progresses to the malignant state, and the emergence of a dominant clone indicates disease progression in ATL [19,20]. As shown in Figure 2B–D, major bands suggesting dominant clones were evident in patients with progressed clinical subtypes or those in the advanced group in the CD3 versus CD7 profile, and major bands existed exclusively in the D and L subpopulations. These data also support the idea that increases in the D and L subpopulations correlate with the progression of disease stage. AC cases in Group 2 had high HTLV-I proviral loads (>4%; Figure 1B) and clear major bands were observed by inverse long PCR in these cases (Figure 2B, right). Sasaki *et al.* reported that two cases of HTVL-I AC with oligoclonal bands on Southern blots and high VLs (20%) had progressed to ATL by 4 and 3.5 years later [21]. The two cases may correspond to HTLV-I AC in Group 2 proposed in our study. In fact, two cases of ACs in our series that were included in Group 2 progressed to smoldering ATL (Figure 4A). AC cases in Group 2 could be regarded as advanced carriers. Our flow cytometric analysis could apparently discriminate high-risk AC cases from stable ones. Follow-up analysis of these cases is warranted to determine whether AC cases included in Group 2 progress to ATL. Flow cytometric data for these AC cases included in Group 2 (Figure 1A and 1C) were similar to those for indolent ATL cases in Group 2. These ACs in Group 2 can be considered essentially the same as smoldering ATL cases. Some of the ACs categorized according to Shimoyama's criteria should in fact be separated and regarded as a subtype together with at least some of the smoldering ATL cases.

Iwanaga *et al.* reported that high HTLV-I proviral load (>4%) in whole PBMCs was a risk factor for progression to ATL [13]. In Figure 1B, the ACs with VLs>4% were distributed between Groups 1 and 2. These findings suggest that not all ACs with high VLs are currently in an advanced stage, although they may have the potential to develop ATL in the future.

In general, the categorization by flow cytometric profile correlated well with the current classification of clinical subtypes, with some exceptional cases of acute-type and smoldering-type disease (Figure 3). The only manifestation of three smoldering cases categorized in Group 1 was skin lesions; they fell into Group 1 because they showed minimal abnormalities in peripheral blood [22]. Three acute-type ATL cases categorized in Group 2 had indolent clinical courses. A diagnosis of acute-type disease is made when the indolent-type and lymphoma-type are excluded, according to Shimoyama's criteria. The CD3 versus CD7 plot may discriminate the cases that will follow an indolent clinical course from the aggressive acute-type ATL.

The VL in each subpopulation indicated that HTLV-I-infected cells were relatively concentrated in the D and L subpopulations (representative data are shown in Figure 2A). These data are consistent with downregulation of CD3 and CD7 being relevant to HTLV-I infection, although cells without HTLV-I infection may also contribute to this change to some extent, as a substantial subpopulation of T cells has been reported to be CD7-deficient under physiological [23,24] and certain pathological conditions,

including autoimmune disorders and viral infection [25–29]. To more precisely analyze phenotypic changes in HTLV-I-infected cells, markers that indicate HTLV-I infection should be incorporated in future studies.

A summary of this study is shown in Figure 5. In the CD3 versus CD7 profile, most AC cases were included in Group 1, in which the D and L subpopulations were relatively small. Consistent with disease progression to smoldering- and chronic-type ATL, a decrease in the H subpopulation and increases in the D and L subpopulations occur (Group 2). In this step, increases in the sizes of clones in the D and L subpopulations are observed. Further expansion of the leukemic clone results in progression to acute-type ATL in which the L subpopulation has expanded (Group 3). According to a study by Yamaguchi *et al.*, the natural course of ATL is to progress from the HTLV-I carrier state through the intermediate state, smoldering ATL, and chronic ATL, and finally to the acute ATL, indicating a process of multistage leukemogenesis [19]. We consider this study to successfully link the progressive clinical status and phenotypic changes in HTLV-I-infected cells. However, the way in which this profile reflects multistep oncogenesis in HTVL-I infection at the molecular level remains unclear. Further molecular analyses of the three subpopulations will help in understanding the mechanism(s).

Supporting Information

Figure S1 Representative flow cytometric analysis of an HTLV-I asymptomatic carrier (patient no. 32). The CD3 versus CD7 plot of $CD4^+$ cells was constructed according to the gating procedure shown in this figure. In the plot, we designated three subpopulations: H ($CD3^{high}CD7^{high}$), D ($CD3^{dim}CD7^{dim}$), and L ($CD3^{dim}CD7^{low}$).
(PPTX)

Figure S2 A two-dimensional plot of 10 normal controls showing the percentage of the D and L subpopulations.
(PPTX)

Figure S3 Southern blot analysis of clonal integration of the HTLV-I provirus. Representative data (AC, No. 34) are shown. In *Eco*RI or *Pst*I digestion, a band indicated by a red arrow represents the monoclonal integration of the provirus. The band pattern indicates that two major clones coexist. This analysis was performed by a commercial laboratory (SRL, Tokyo, Japan).
(PPTX)

Table S1 Clinical data in a case of chronic-type ATL (No. 53). Proportion of abonormal lymphocytes in the preipheral blood WBC were evaluated by morphological exmanination. LDH: Lactate dehydrogenase (normal range, 120–240 U/L) sIL-2R: soluble interleukin-2 receptor (normal range, 122–496 U/ml).
(XLSX)

Acknowledgments

We thank Dr. Toshiki Watanabe, Dr. Kazumi Nakano, and Dr. Tadanori Yamochi (The University of Tokyo) for providing the TL-Om1 cell line and the plasmid containing the HTLV-I genome, which was used as a standard for the quantification of proviral load. We also thank Mr. Yuji Zaike (Clinical Laboratory, Research Hospital, Institute of Medical Science, The University of Tokyo) for his excellent technical advice. We are grateful to the hospital staff who have made a commitment to providing high-quality care to all of our patients.

Author Contributions

Conceived and designed the experiments: KT AT KU. Performed the experiments: SK YT. Analyzed the data: EW NW TI NO. Contributed reagents/materials/analysis tools: MI MT KU NO. Wrote the paper: SK KU.

References

1. Yoshida M, Miyoshi I, Hinuma Y (1982) Isolation and characterization of retrovirus from cell lines of human adult T-cell leukemia and its implication in the disease. Proc Natl Acad Sci U S A 79: 2031–2035.
2. Osame M, Usuku K, Izumo S, Ijichi N, Amitani H, et al. (1986) HTLV-I associated myelopathy, a new clinical entity. Lancet 1: 1031–1032.
3. Mochizuki M, Watanabe T, Yamaguchi K, Takatsuki K, Yoshimura K, et al. (1992) HTLV-I uveitis: a distinct clinical entity caused by HTLV-I. Japanese journal of cancer research : Gann 83: 236–239.
4. Proietti FA, Carneiro-Proietti AB, Catalan-Soares BC, Murphy EL (2005) Global epidemiology of HTLV-I infection and associated diseases. Oncogene 24: 6058–6068.
5. Yamaguchi K, Watanabe T (2002) Human T lymphotropic virus type-I and adult T-cell leukemia in Japan. International journal of hematology 76 Suppl 2: 240–245.
6. Murphy EL, Hanchard B, Figueroa JP, Gibbs WN, Lofters WS, et al. (1989) Modelling the risk of adult T-cell leukemia/lymphoma in persons infected with human T-lymphotropic virus type I. International journal of cancer Journal international du cancer 43: 250–253.
7. Shimoyama M (1991) Diagnostic criteria and classification of clinical subtypes of adult T-cell leukaemia-lymphoma. A report from the Lymphoma Study Group (1984–87). Br J Haematol 79: 428–437.
8. Tsukasaki K, Hermine O, Bazarbachi A, Ratner L, Ramos JC, et al. (2009) Definition, prognostic factors, treatment, and response criteria of adult T-cell leukemia-lymphoma: a proposal from an international consensus meeting. J Clin Oncol 27: 453–459.
9. Takasaki Y, Iwanaga M, Imaizumi Y, Tawara M, Joh T, et al. (2010) Long-term study of indolent adult T-cell leukemia-lymphoma. Blood 115: 4337–4343.
10. Hisada M, Okayama A, Shioiri S, Spiegelman DL, Stuver SO, et al. (1998) Risk factors for adult T-cell leukemia among carriers of human T-lymphotropic virus type I. Blood 92: 3557–3561.
11. Imaizumi Y, Iwanaga M, Tsukasaki K, Hata T, Tomonaga M, et al. (2005) Natural course of HTLV-1 carriers with monoclonal proliferation of T lymphocytes ("pre-ATL") in a 20-year follow-up study. Blood 105: 903–904.
12. Kamihira S, Atogami S, Sohda H, Momita S, Yamada Y, et al. (1994) Significance of soluble interleukin-2 receptor levels for evaluation of the progression of adult T-cell leukemia. Cancer 73: 2753–2758.
13. Iwanaga M, Watanabe T, Utsunomiya A, Okayama A, Uchimaru K, et al. (2010) Human T-cell leukemia virus type I (HTLV-1) proviral load and disease progression in asymptomatic HTLV-1 carriers: a nationwide prospective study in Japan. Blood 116: 1211–1219.
14. Okamoto T, Ohno Y, Tsugane S, Watanabe S, Shimoyama M, et al. (1989) Multi-step carcinogenesis model for adult T-cell leukemia. Japanese journal of cancer research : Gann 80: 191–195.
15. Matsuoka M, Jeang KT (2007) Human T-cell leukaemia virus type 1 (HTLV-1) infectivity and cellular transformation. Nat Rev Cancer 7: 270–280.
16. Yoshida M (2010) Molecular approach to human leukemia: isolation and characterization of the first human retrovirus HTLV-1 and its impact on tumorigenesis in adult T-cell leukemia. Proceedings of the Japan Academy Series B, Physical and biological sciences 86: 117–130.
17. Tian Y, Kobayashi S, Ohno N, Isobe M, Tsuda M, et al. (2011) Leukemic T cells are specifically enriched in a unique CD3(dim) CD7(low) subpopulation of CD4(+) T cells in acute-type adult T-cell leukemia. Cancer science 102: 569–577.
18. Sugamura K, Fujii M, Kannagi M, Sakitani M, Takeuchi M, et al. (1984) Cell surface phenotypes and expression of viral antigens of various human cell lines carrying human T-cell leukemia virus. International journal of cancer Journal international du cancer 34: 221–228.
19. Yamaguchi K, Kiyokawa T, Nakada K, Yul LS, Asou N, et al. (1988) Polyclonal integration of HTLV-I proviral DNA in lymphocytes from HTLV-I seropositive individuals: an intermediate state between the healthy carrier state and smouldering ATL. British journal of haematology 68: 169–174.
20. Mortreux F, Gabet AS, Wattel E (2003) Molecular and cellular aspects of HTLV-1 associated leukemogenesis in vivo. Leukemia : official journal of the Leukemia Society of America, Leukemia Research Fund, UK 17: 26–38.
21. Sasaki D, Doi Y, Hasegawa H, Yanagihara K, Tsukasaki K, et al. (2010) High human T cell leukemia virus type-1(HTLV-1) provirus load in patients with HTLV-1 carriers complicated with HTLV-1-unrelated disorders. Virology journal 7: 81.
22. Setoyama M, Katahira Y, Kanzaki T (1999) Clinicopathologic analysis of 124 cases of adult T-cell leukemia/lymphoma with cutaneous manifestations: the smouldering type with skin manifestations has a poorer prognosis than previously thought. The Journal of dermatology 26: 785–790.
23. Reinhold U, Abken H (1997) CD4+ CD7- T cells: a separate subpopulation of memory T cells? J Clin Immunol 17: 265–271.

24. Reinhold U, Abken H, Kukel S, Moll M, Muller R, et al. (1993) CD7- T cells represent a subset of normal human blood lymphocytes. J Immunol 150: 2081–2089.
25. Aandahl EM, Quigley MF, Moretto WJ, Moll M, Gonzalez VD, et al. (2004) Expansion of CD7(low) and CD7(negative) CD8 T-cell effector subsets in HIV-1 infection: correlation with antigenic load and reversion by antiretroviral treatment. Blood 104: 3672–3678.
26. Autran B, Legac E, Blanc C, Debre P (1995) A Th0/Th2-like function of CD4+CD7- T helper cells from normal donors and HIV-infected patients. J Immunol 154: 1408–1417.
27. Legac E, Autran B, Merle-Beral H, Katlama C, Debre P (1992) CD4+CD7-CD57+ T cells: a new T-lymphocyte subset expanded during human immunodeficiency virus infection. Blood 79: 1746–1753.
28. Schmidt D, Goronzy JJ, Weyand CM (1996) CD4+ CD7- CD28- T cells are expanded in rheumatoid arthritis and are characterized by autoreactivity. J Clin Invest 97: 2027–2037.
29. Willard-Gallo KE, Van de Keere F, Kettmann R (1990) A specific defect in CD3 gamma-chain gene transcription results in loss of T-cell receptor/CD3 expression late after human immunodeficiency virus infection of a CD4+ T-cell line. Proc Natl Acad Sci U S A 87: 6713–6717.

High-grade Lung Adenocarcinoma With Fetal Lung–like Morphology

Clinicopathologic, Immunohistochemical, and Molecular Analyses of 17 Cases

Shigeki Morita, MD,† Akihiko Yoshida, MD, PhD,*† Akiteru Goto, MD, PhD,† Satoshi Ota, MD, PhD,† Koji Tsuta, MD, PhD,* Karin Yokozawa, BSc,* Hisao Asamura, MD, PhD,‡ Jun Nakajima, MD, PhD,§ Daiya Takai, MD, PhD,‖ Masaya Mori, MD, PhD,¶ Teruaki Oka, MD,# Junichi Tamaru, MD, PhD,# Shinji Itoyama, MD, PhD,# Koh Furuta, MD, PhD,* Masashi Fukayama, MD, PhD,† and Hitoshi Tsuda, MD, PhD**

Abstract: Low-grade lung adenocarcinoma of fetal lung type, which is well characterized by its unique clinicopathologic and molecular features, is recognized as a distinct variant of lung cancer. In contrast, high-grade lung adenocarcinoma with fetal lung–like morphology (HG-LAFM) has not been studied widely. To characterize this subset better, we analyzed 17 high-grade adenocarcinomas with at least focal component resembling a developing epithelium in the pseudoglandular phase of the fetal lung. These rare (ca. 0.4%) carcinomas occurred predominantly in elderly men with a heavy smoking history, who showed elevated serum α-fetoprotein in 4 of 5 cases tested. Histologic examination revealed a fetal lung–like component as a focal finding accounting for 5% to 60% of the total tumor volume. It was invariably admixed with tissues having a morphology not resembling that of a fetal lung. A coexisting non–fetal lung–like element was quite heterogenous in appearance, showing various growth patterns. However, clear-cell (88%), hepatoid (29%), and large cell neuroendocrine carcinoma (24%) histology seemed overrepresented. HG-LAFM was characterized immunohistochemically by frequent expression of α-fetoprotein (41%), glypican-3 (88%), SALL-4 (59%), neuroendocrine markers (82%), CDX-2 (35%), and p53 (65%). HG-LAFM was molecularly heterogenous in that *EGFR* or *KRAS* mutation was observed in 22% of cases tested for both. Our data indicate that HG-LAFMs might form a coherent subgroup of lung adenocarcinomas. However, the uniformly focal nature of the fetal lung–like element, widely diverse coexisting non–fetal lung–like histology, and inhomogenous molecular profiles lead us to believe that HG-LAFM is best regarded as a morphologic pattern showing characteristic association with several clinicopathologic parameters rather than a specific tumor entity.

Key Words: lung, adenocarcinoma, fetal, neuroendocrine

(*Am J Surg Pathol* 2013;37:924–932)

Lung cancer is the leading cause of tumor mortality worldwide.[1] Adenocarcinoma, the most common subtype, is well known for its diverse morphologic appearance.[2] Primary lung adenocarcinomas can, but rarely, exhibit morphologic features resembling those of a developing fetal lung.[3–8] In 1998, Nakatani et al[8] reviewed 16 lung carcinomas with such features and subdivided them into low-grade and high-grade forms. Low-grade adenocarcinoma of fetal lung type (also known as pulmonary endodermal tumor resembling fetal lung[4]) was characterized by complex glandular structures resembling a developing epithelium in the pseudoglandular phase of the fetal lung, low nuclear atypia, and morule formation. In contrast, aside from the fetal lung–like epithelial character, the high-grade form was found to show prominent nuclear atypia, a lack of morules, a transition to conventional adenocarcinoma, and necrosis. This dichotomous classification was later applied to biphasic tumors conventionally known as "pulmonary blastoma." They were subdivided into "classic" type associated with low-grade fetal lung–like epithelium and "blastomatoid variant of carcinosarcoma" associated with high-grade fetal lung–like epithelium.[9]

Subsequent molecular studies have revealed that the low-grade adenocarcinoma of fetal lung type (and its biphasic variant) was characterized by β-catenin gene mutation leading to aberrant nuclear/cytoplasmic β-catenin

From the Departments of *Pathology and Clinical Laboratories; ‡Thoracic Oncology, Thoracic Surgery Division, National Cancer Center Hospital; †Department of Pathology, Graduate School of Medicine, The University of Tokyo; Departments of §Thoracic Surgery; ‖Clinical Laboratory, The University of Tokyo Hospital; ¶Mitsui Memorial Hospital, Tokyo; and #Department of Pathology, Saitama Medical Center, Saitama Medical University, Saitama, Japan.

Conflicts of Interest and Source of Funding: The authors have disclosed that they have no significant relationships with, or financial interest in, any commercial companies pertaining to this article.

Correspondence: Masashi Fukayama, MD, PhD, Department of Pathology, Graduate School of Medicine, The University of Tokyo, 7-3-1 Hongo, Bunkyo-ku, Tokyo 113-0033, Japan (e-mail: mfukayama-tky@umin.net).

expression.[9–11] Currently, low-grade adenocarcinoma of fetal lung type is recognized as a distinct subgroup of lung cancer in the current World Health Organization (WHO) classification by the name of well-differentiated fetal adenocarcinoma.[2] In contrast, the high-grade form, hereinafter termed high-grade lung adenocarcinoma with fetal lung–like morphology (HG-LAFM) in this article, has not been investigated widely. No systematic study of this subset has been undertaken since the original proposal by Nakatani et al,[8] and it remains unclear whether HG-LAFM is a distinct variant of lung cancer.

In this study, we examined clinicopathologic, immunohistochemical, and molecular features of 17 cases of HG-LAFM retrospectively to elucidate this morphologic subset and to determine whether HG-LAFM deserves designation as a specific variant of lung adenocarcinoma.

MATERIALS AND METHODS

Case Selection

This study was approved by the review board of each participating institution. HG-LAFMs were sought electronically from the respective surgical pathology archives of the National Cancer Center Hospital (Tokyo), The University of Tokyo Hospital (Tokyo), Mitsui Memorial Hospital (Tokyo), and Saitama Medical University (Saitama). The search was facilitated by key words such as "fetal," "primitive," and "immature." Fetal lung–like morphology was defined by complex glandular architecture composed of tall columnar cells that displayed supranuclear and/or subnuclear clear cytoplasm resembling a developing epithelium in the pseudoglandular phase of the fetal lung. Occasional papillary infoldings were allowed. The oval-shaped nucleus in each constituent tumor cell was typically aligned as perpendicular to the basement membrane. The apical border of tumoral glands was flat rather than interrupted by apical snouts. The nuclear grade was high. We required at least focal area of unequivocal fetal lung–like morphology for inclusion in this study. Two low-grade adenocarcinomas of fetal lung type (1 monophasic and 1 biphasic) in the archives were excluded. The search ultimately identified 17 cases of HG-LAFM, which accounted for ca. 0.4% of the >4000 primary lung cancer cases that had been surgically resected at the participating institutions.

Clinicopathologic Examination

Medical records were reviewed for demographic data, smoking history, serum α-fetoprotein (AFP) level when available, and follow-up information. Tumors were staged according to the TNM system.[12] All the tumors had been sampled adequately, fixed in 10% formalin, embedded in paraffin, cut into 4-μm-thick sections, and stained with hematoxylin and eosin for routine pathologic examination. All available glass slides were reviewed by 2 or 3 pathologists (S.M., A.G., and A.Y.). The amount of fetal lung–like element was evaluated as a percentage of the total tumor volume. Coexisting components that did not resemble developing fetal lung were also assessed and were classified on the basis of WHO guidelines.[2] The conventional adenocarcinoma component was characterized further by the growth pattern (lepidic, papillary, acinar, and solid) according to a recent recommendation.[13] In addition, we devoted attention to the presence or absence of hepatoid and clear-cell patterns and recorded these patterns separately. Although unrecognized in the present WHO scheme, a hepatoid pattern in lung adenocarcinoma was previously documented[14–17] and was defined by solid to trabecular growth of tumor cells having eosinophilic cytoplasm, thereby simulating hepatocellular carcinoma. A clear-cell pattern indicated tumor cells showing significantly clear cytoplasm irrespective of the growth pattern.[18] Because fetal lung–like tumor cells harbored clear cytoplasm by definition, we considered only non–fetal lung–like element with clear cytoplasm as a clear-cell pattern for evaluation. The relative amount of each non–fetal lung–like histologic pattern was expressed as a percentage of the total tumor volume. Lymphovascular invasion, pleural invasion, and necrosis were assessed. Metastatic tumor tissues in lymph nodes were also evaluated when available.

Immunohistochemistry

For immunohistochemical staining, primary antibodies for AFP, glypican-3 (GPC-3), SALL-4, synaptophysin, chromogranin A, neural cell adhesion molecule, thyroid transcription factor-1 (TTF-1), CDX-2, p53, and β-catenin were used (Table 1). Sections of 4 μm thickness from each block of the tumor tissue were stained using an automated stainer (Ventana Benchmark; Ventana Medical Systems Inc., Tucson, AZ) along with appropriate positive and negative controls.

All samples were evaluated and scored by 2 pathologists (S.M. and A.G.) without knowledge of clinicopathologic data. Staining of >1% of tumor cells was required for the positive designation except for p53, in which nuclear staining of >10% of tumor cells was considered positive.

Molecular Analysis

We performed a mutation analysis of epidermal growth factor receptor (*EGFR*) to detect deletion in exon 19 and point mutation in exon 21 (L858R) and of *KRAS* exon 2 (codons 12 and 13) and exon 3 (codon 61) by high-resolution melting analysis. DNA was extracted from archived formalin-fixed or methanol-fixed, paraffin-embedded tissues using the QIAamp DNA Micro Kit (Qiagen Inc., Valencia, CA), following the manufacturer's instructions. Polymerase chain reaction was performed to amplify exons 19 and 21 of *EGFR* and exons 2 and 3 of *KRAS* using LCGreen I (Idaho Technology, Salt Lake City, UT) on a thermal cycler. Primers for *EGFR* analysis were designed as described previously.[19] Primers for *KRAS* exon 3 analysis were commercially available (Idaho Technology), and primers for *KRAS* exon 2 (92 bp) were published previously by others.[20] An additional set of primers for *KRAS* exon 2 (62 bp) was

TABLE 1. Antibodies Used for Immunohistochemical Studies

Antibody	Clone	Type	Source	Dilution	Staining Pattern
AFP	—	Rabbit, poly	Dako, Glostrup, Denmark	1:1000	C
GPC-3	1G12	Mouse, mono	BioMosaics Inc., Burlington, VT	1:200	C, M
SALL-4	6E3	Mouse, mono	Abnova Corp., Taipei, Taiwan	1:100	N
Synaptophysin	—	Rabbit, poly	Dako	1:100	C
Chromogranin A	—	Rabbit, poly	Dako	1:200	C
NCAM (CD56)	1B6	Mouse, mono	Novocastra Laboratories Ltd., Newcastle, UK	1:50	M
TTF-1	8G7G3/1	Mouse, mono	Neomarkers, Fremont, CA	1:200	N
CDX-2	CDX-2-88	Mouse, mono	BioGenex, San Ramon, CA	1:50	N
p53	DO-7	Mouse, mono	Novocastra Laboratories Ltd.	1:100	N
β-catenin	14/ β-catenin	Mouse, mono	BD Transduction Laboratories, San Diego, CA	1:1000	N

C indicates cytoplasmic; M, membranous; N, nuclear; NCAM, neural cell adhesion molecule; poly, polyclonal; mono, monoclonal; TTF-1, thyroid transcription factor-1.

designed by one of the authors (K.Y.). The primer sequences are presented in Table 2. These polymerase chain reaction products were analyzed using the LightScanner platform (Idaho Technology). Data were acquired and analyzed using the accompanying software (Idaho Technology). After the normalization step, melting curve shapes of the tumor samples and control samples were compared. Human Genomic DNA (Roche Diagnostics Corp., Indianapolis, IN) was used as the negative control sample with wild-type *EGFR* and *KRAS*. All analyses were performed in a blinded manner to the clinicopathologic data.

Statistics

Three-year and 5-year overall survival and disease-free survival rates were calculated with the Kaplan-Meier method using software STAT View for Windows, ver. 5 (SAS Institute Inc., Cary, NC).

RESULTS

Clinical Characteristics

The clinical characteristics of HG-LAFMs are presented in Table 3. HG-LAFM almost exclusively occurred in men (16 men, 1 woman). The patient ages ranged from 40 to 75 years (median, 64.2 y). Except for 2 patients whose smoking history was unknown, all the patients had been heavy smokers with exposure of >20 pack-years (median, 54.9 p-y). Three patients were symptomatic at presentation with cough (cases 3 and 4) or chest pain (case 1). Serum AFP level was available in 5 cases, and it was elevated in 4 of them (case 8, 8720 ng/mL; case 12, 19 ng/mL; case 13, 16 ng/mL; case 17, 24 ng/mL, normal range: <10 ng/mL). All patients were treated with lobectomy and standard lymph node dissection with a curative intent. No postoperative complication was recorded. Nine patients received postoperative chemotherapy. None received preoperative chemotherapy. The pathologic stages were I in 7, II in 6, and III in 4 cases. Follow-up data were available for all patients with duration of 1 to 85 months (median, 29.3 mo). Six patients developed distant metastases (case 1, adrenal; case 5, adrenal and bone; case 6, brain; case 10, brain and adrenal; case 11, lung; case 12, liver), and an additional patient had a metastasis to hilar lymph nodes (case 14) after surgery. Three-year and 5-year disease-free survival rates were 48.6% and 48.6%, respectively, and 3-year and 5-year overall survival rates were 71.4% and 53.6%, respectively.

Histopathologic Findings

The histologic characteristics of HG-LAFMs are presented in Table 3 and are shown in Figure 1. The tumors measured 1.9 to 9.5 cm (average, 5.0 cm). All the

TABLE 2. *EGFR* and *KRAS* High-Resolution Melting Analysis Primer Sequences

Exon	Primer Name	Sequence	Amplicon Size
21 (L858R)	*EGFR*_ex18_F	5′-AGATCACAGATTTTGGGC-3′	51 bp
	*EGFR*_ex18_R	5′-ATTCTTTCTCTTCCGCAC-3′	
19 (deletion)	*EGFR*_ex19_F	5′-AAAATTCCCGTCGCTATC-′3	83 bp
	*EGFR*_ex19_R	5′-AAGCAGAAACTCACATCG-′3	
2 (189 bp)	*KRAS* (codon12, 13, 189 bp)_ex2_F	5′-TCATTATTTTTATTATAAGGCCTGCTGAA-3′	189 bp
	KRAS (codon12, 13, 189 bp)_ex2_R	5′-CAAAGACTGGTCCTGCACCAGTA-3′	
2 (92 bp)	*KRAS* (codon12, 13, 92 bp)_ex2_F	5′-TTATAAGGCCTGCTGAAAATGACTGAA-3′	92 bp
	KRAS (codon12, 13, 92 bp)_ex2_R	5′-TGAATTAGCTGTATCGTCAAGGCACT-3′	
2 (62 bp)	*KRAS* (codon12, 13, 62 bp)_ex2_F	5′-TAAACTTGTGGTAGTTGGAGC-3′	62 bp
	KRAS (codon12, 13, 62 bp)_ex2_R	5′-GAATTAGCTGTATCGTCAAGG-3′	
3 (codon 61)	*KRAS* (codon61)_ex3_F	5′-CACTGTAATAATCCAGACTGTGTTTC-3′	266 bp
	KRAS (codon61)_ex3_R	5′-AACTATAATTACTCCTTAATGTCAGCTT-3′	

TABLE 3. Clinical and Histopathologic Features of 17 High-grade Lung Adenocarcinomas with Fetal Lung–like Morphology

						Histologic Patterns						
Case	Age (y)	Sex	Smoking (p-y)	Size (cm)	Stage	Fetal (%)	Hep (%)	Clear (%)	LCNEC (%)	Others (%)	Histology in LN Metastasis	Follow-up (mo)
1	61	M	91	8.0	IIIA	60	—	15	—	Aci 20, pap 5	Aci, pap, fetal	DOD (55)
2	70	M	37.5	1.9	IA	50	—	—	—	Lep 30, pap 10, aci 10	—	NED (85)
3	67	M	47	5.0	IB	20	10	20	45	Pap 5	—	NED (61)
4	69	M	37	3.8	IB	30	—	35	10	Pap 10, aci 10, lep 5	—	NED (48)
5	73	M	55	5.5	IB	5	—	—	—	Aci 65, pap 15, lep 10, sol 5	—	AWD (15)
6	65	M	45	4.5	IIB	20	—	20	20	Aci 20, pap 10, lep 10	LCNEC	DOD (26)
7	58	M	114	3.5	IIB	15	30	45	—	Aci 10	—	NED (13)
8	53	M	45	7.3	IIB	5	5	10	60	Aci 20	—	NED (12)
9	62	F	21	5.5	IB	10	40	10	—	Aci 10, pap 10, sol 20	—	NED (12)
10	40	M	50	6.5	IIIA	30	—	25	—	Pap 20, aci 15, sol 10	Aci, fetal	AWD (24)
11	65	M	NA	6.5	IIIA	15	—	15	—	Aci 40, pap 20, sol 10	Fetal, clear, pap	DOD (21)
12	69	M	49	4.5	IIB	30	—	60	—	Pap 10	Pap	DOD (9)
13	55	M	28	4.0	IIIB	20	—	20	—	Aci 40, pap 10, sol 5, lep 5	—	NED (26)
14	74	M	100	3.0	IIB	5	25	50	—	Sol 10, aci 10	Sol, fetal, clear	AWD (12)
15	73	M	40	9.5	IB	30	—	15	—	Aci 20, lep 20, pap 10, sol 5	—	NED (18)
16	75	M	NA	3.2	IB	45	—	15	—	Pap 40	—	NED (60)
17	62	M	63	3.5	IIB	40	—	20	—	Pap 20, aci 15, sol 5	—	NED (1)

Aci indicates acinar pattern; AWD, alive with disease; clear, clear-cell; DOD, died of disease; F, female; fetal, fetal lung–like; hep, hepatoid; lep, lepidic pattern; LN, lymph node, M, male; NA, data not available; NED, no evidence of disease; pap, papillary pattern; sol, solid pattern.

17 tumors showed at least focal area resembling fetal lung epithelium by selection criteria (Figs. 1A, B). The fetal lung–like component accounted for 5% to 60% (average, 25%) of the total tumor volume. None of the 17 tumors consisted entirely of fetal lung–like morphology. No tumor showed morule formation. The coexisting non–fetal lung–like components consisted of conventional adenocarcinoma that displayed various patterns including lepidic (6 cases, 35%), papillary (14 cases, 82%), acinar (14 cases, 82%), and solid (8 cases, 47%) patterns (Fig. 1C). In addition to such conventional patterns, a hepatoid pattern was identified in 5 cases (29%, Fig. 1D) and clear-cell component (exclusive of fetal lung–like element) was observed in 15 cases (88%; Fig. 1E). Four cases had a large cell neuroendocrine carcinoma (LCNEC) component (cases 3, 4, 6, and 8; Fig. 1F). None of the 17 cases harbored squamous cell or small cell differentiation. None was a biphasic tumor with sarcomatoid element. Lymphovascular and pleural invasions were identified in 14 and 11 cases, respectively. Necrosis was identified in all cases, and 13 cases (76%) showed grossly visible massive necrosis. Lymph node metastasis was identified in 6 cases (35%), of which 4 lesions showed fetal lung–like morphology.

Immunohistochemical Findings

Immunostaining results are presented in Figures 2 and 3. Both fetal lung–like and coexisting non–fetal lung–like components were often positive for oncofetal proteins such as AFP (Fig. 3A), GPC-3 (Fig. 3B), and SALL-4 (Fig. 3C). These oncofetal proteins were more frequently positive in the non–fetal lung–like component, particularly in the clear-cell and hepatoid patterns, than in the fetal lung–like component. Specifically, the fetal lung–like component was positive for AFP, GPC-3, and SALL-4 in 29%, 76%, and 53%, respectively, whereas the non–fetal lung–like component labeled for these markers in 41%, 88%, and 59%, respectively. Similarly, at least 1 of 3 neuroendocrine markers (ie, synaptophysin, chromogranin A, and neural cell adhesion molecule) was positive in most (82%) cases, and it was more frequently positive in the non–fetal lung–like component (82%) than in the fetal lung–like component (65%) (Fig. 3D). Thyroid transcription factor-1, CDX-2, and p53 were positive in 41%, 35%, and 59% of fetal lung–like components, respectively; they were positive in 53%, 35%, and 65% of non–fetal lung–like component, respectively (Figs. 3E, F). No nuclear or cytoplasmic aberrant expression of β-catenin was observed in any of the 17 cases.

Molecular Characteristics

Molecular characteristics of HG-LAFMs are presented in Table 4. Mutation analyses of *EGFR* and *KRAS* genes were performed in 14 and 9 cases, respectively. One case harbored L858R mutation of *EGFR*, and another showed *KRAS* mutation in either codon 12 or 13. The remaining cases tested were of wild type for both *EGFR* and *KRAS*.

DISCUSSION

This comprehensive study of HG-LAFMs clarified their clinicopathologic characteristics and highlighted its difference from the reported traits of low-grade adenocarcinoma of fetal lung type.[8,11] In addition to an unfavorable prognosis inherently attached to high tumor grade, the differences include the following. First,

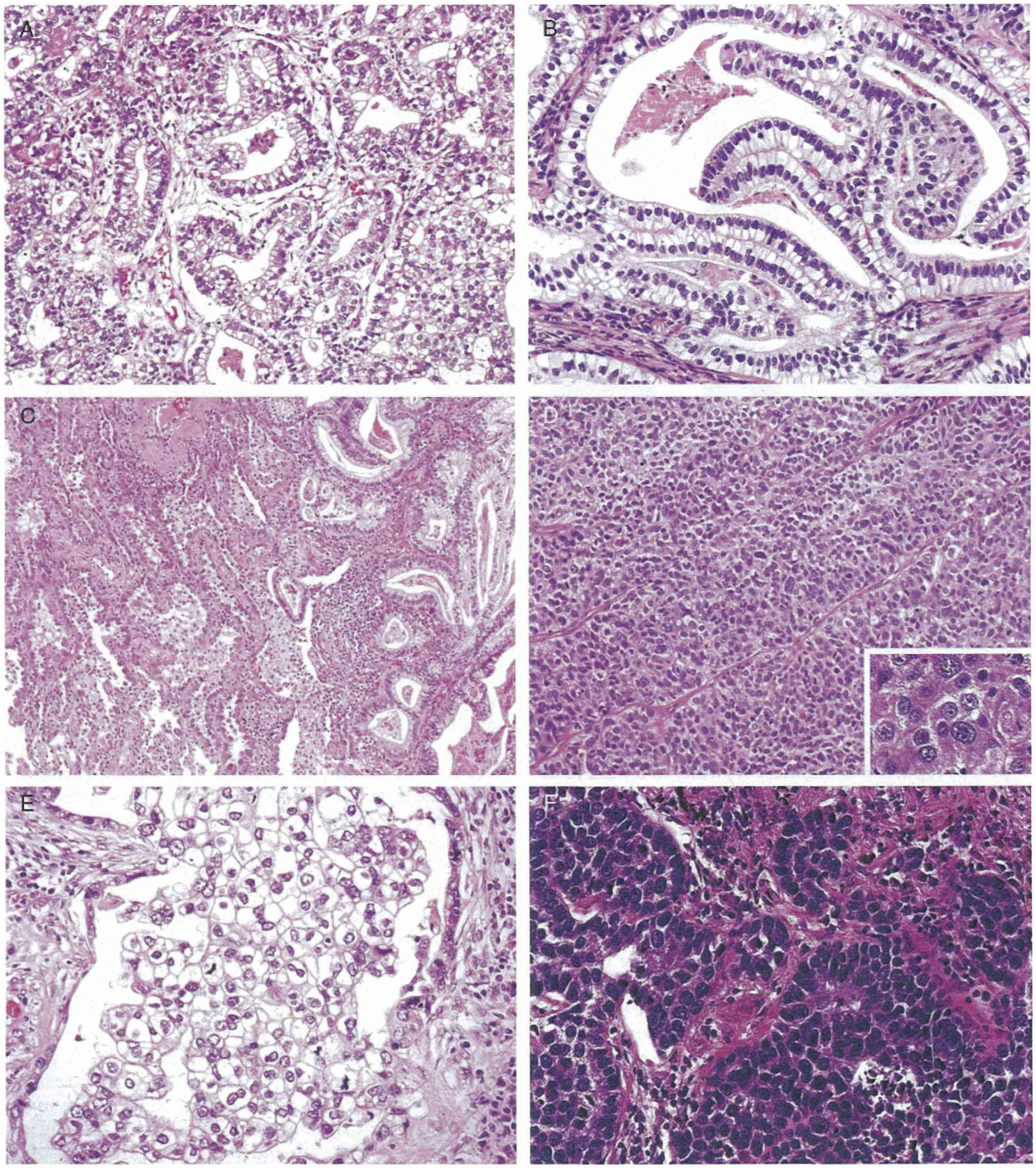

FIGURE 1. HG-LAFM showed at least focal element that resembles developing fetal lung (A and B), in which columnar cells with supranuclear or subnuclear cytoplasmic clearing displayed complex glandular architecture. Fetal lung–like component was invariably accompanied by conventional adenocarcinoma (C, right: fetal lung–like pattern; left: conventional pattern). Hepatoid (D, inset shows a magnified view of hepatoid cells) and clear-cell patterns (E) were overrepresented in non–fetal lung–like component. HG-LAFM was combined with LCNEC in 4 cases (F).

HG-LAFMs predominantly occurred in old men with a consistent heavy smoking history, unlike low-grade carcinoma, which develops in younger patients with a female predominance.[5,8,10,21] Second, a fetal lung–like component in HG-LAFMs was invariably a focal finding accompanied by a histology that did not resemble that of a

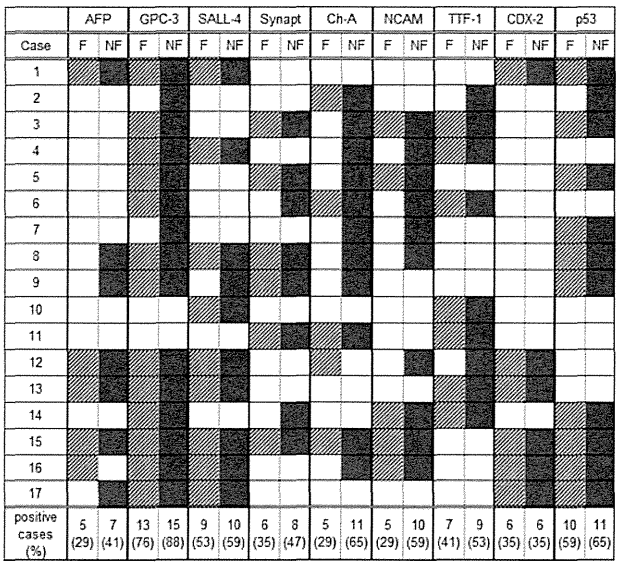

FIGURE 2. Immunoprofiles of 17 HG-LAFMs. The left halves of the 2 boxes for each molecule show the results in fetal lung–like component. The right halves show the result in the co-existing non–fetal lung–like component. A filled box represents positive staining. An empty box means a negative result. F denotes a fetal lung–like component; NF, a non–fetal lung–like component; Synapt, synaptophysin; Ch-A, chromogranin A; NCAM, neural cell adhesion molecule; TTF-1, thyroid transcription factor-1.

fetal lung, whereas low-grade adenocarcinoma of the fetal lung type was reported to manifest typically in a pure fetal lung–like form.[10,11,21] Third, all of our HG-LAFMs lacked morule formation and aberrant immunoexpression of β-catenin, which are 2 signature findings of low-grade adenocarcinoma of the fetal lung type.[10,11] We therefore agree with Nakatani et al[8] that low-grade and high-grade lung adenocarcinomas harboring fetal lung–like morphology are completely different diseases, rather than 2 related tumors in the same family differing only in their grades. In this respect, we believe that the current WHO classification system is somewhat confusing because both low-grade and high-grade tumors are read under the same heading by the name of well-differentiated and poorly differentiated fetal adenocarcinoma, respectively. From a practical standpoint, careful wording is necessary when discussing fetal lung–like morphology in a report of high-grade tumors in order to avoid confusion with low-grade adenocarcinoma. We elected to use HG-LAFM terminology in this report because of the concern that the originally proposed "high-grade adenocarcinoma of fetal lung type"[8] terminology might give an inaccurate impression of its relatedness with low-grade adenocarcinoma of fetal lung type.

Coexisting non–fetal lung–like histology in HG-LAFM was quite heterogenous, and it included all 4 common growth patterns of conventional adenocarcinoma: lepidic, papillary, acinar, and solid patterns. Nonetheless, our data suggest that fetal lung–like differentiation has a peculiar tendency to admix with particular non–fetal lung–like morphologic attributes. Specifically, hepatoid morphology and clear-cell pattern, 2 uncommon phenotypes in lung adenocarcinoma,[14–18] appeared to be overrepresented in the non–fetal lung–like component. These results suggest that fetal lung–like morphology might not be a mere capricious phenotypic variation that any given lung cancer might display, but it might represent a line of differentiation that only a particular subset of lung cancer can undergo.

In agreement with a previous study,[8] we showed that as many as approximately 80% of HG-LAFMs displayed immunohistochemical evidence of neuroendocrine differentiation. Although immunoreactivity to neuroendocrine markers can be seen in 16% to 36% of morphologically nondescript lung adenocarcinomas,[22–24] the rate of positivity appeared high in HG-LAFMs, which suggests a clearer tendency of neuroendocrine differentiation in this tumor subset. Supporting this hypothesis, 4 of 17 HG-LAFMs in our series displayed morphologic evidence of neuroendocrine differentiation in the form of admixture with LCNEC. In no report of the relevant literature has HG-LAFM with LCNEC component been clearly described, although 1 putative example of HG-LAFM[6] was reportedly associated with "carcinoid-like neuroendocrine component," and the latter element might meet the contemporary criteria of LCNEC.

An increased level of serum AFP was identified in 4 of 5 cases tested. Immunohistochemical AFP staining was demonstrated in 8 cases (47%). This observation is consistent with those of a previous study[8] in which 29% of HG-LAFM demonstrated AFP immunoexpression. AFP production in adenocarcinoma was reported in many other organ systems, and it has been documented most commonly in stomach cancers. AFP-producing stomach cancer is known to occur in elderly patients, and it is characterized by prominent vascular invasion and frequent liver metastasis.[25–28] Previous histologic analyses of AFP-producing gastric carcinoma have identified several characteristic morphologic patterns: primitive gut (enteroblastic), hepatoid, clear-cell, and yolk sac tumor like.[26–30] It is particularly interesting that the histology of primitive gut–type (enteroblastic) stomach cancer was described and illustrated as having a complex glandular structure lined by columnar cells with clear cytoplasm.[26–28,30] To a great degree, its morphology overlaps fetal lung–like histology that we describe in lung cancer (compare our Figs. 1A and B with the histology of AFP-producing stomach cancers depicted in Image 2 of Maitra et al,[26] Figure 2 of Kodama et al,[27] Figure 4 of Motoyama et al,[28] and Figure 1 of Matsunou et al[30]). Nakatani et al,[8] in their original series, also recognized this resemblance.

The histologic analogy between lung and stomach cancers is strengthened further by the frequent coexistence of hepatoid and clear-cell patterns in our HG-LAFMs, because these 2 patterns are also common in AFP-producing stomach cancers.[26–32] Immunohistochemical analysis provided yet another support for this parallel, in that

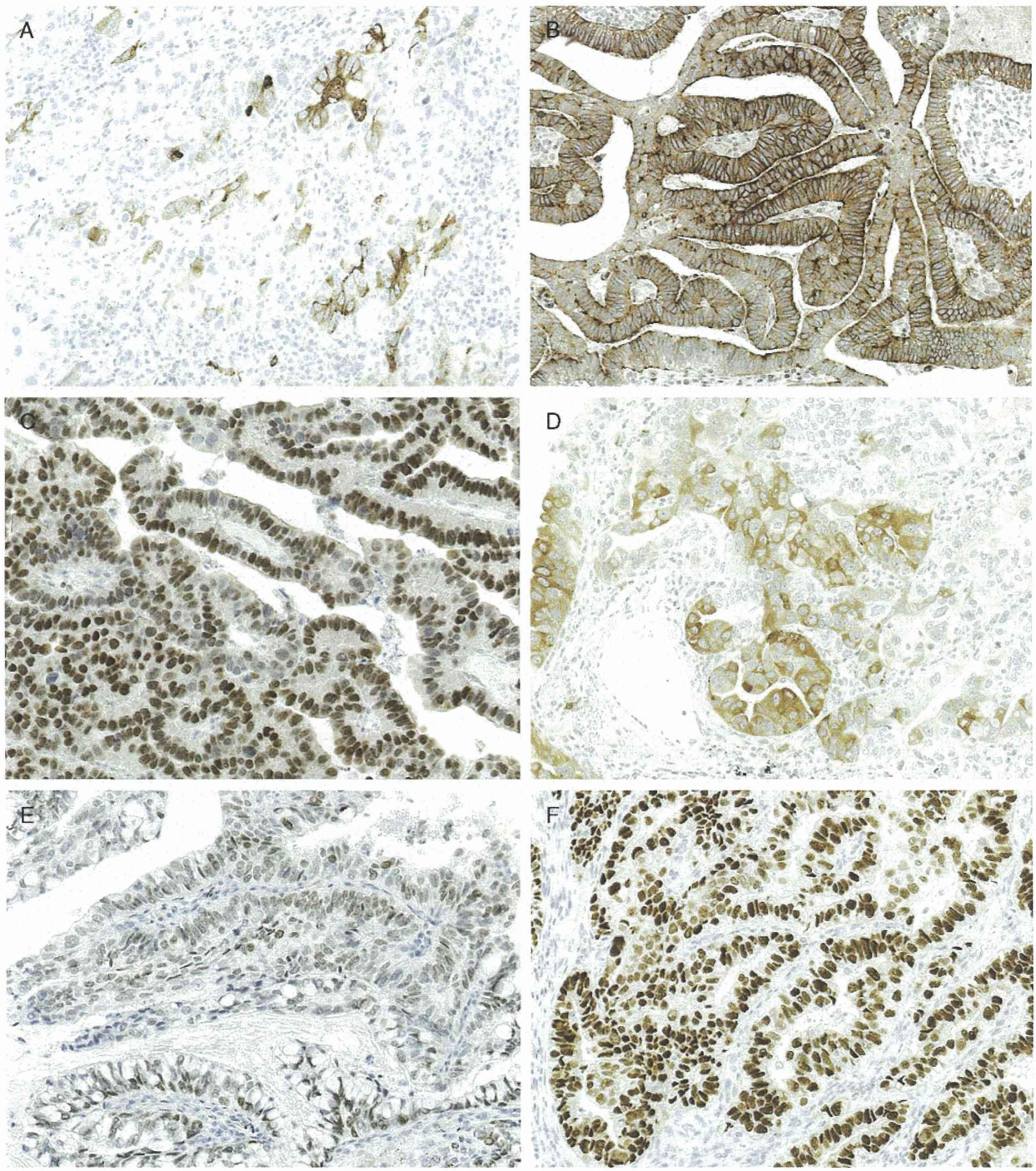

FIGURE 3. Immunohistochemical staining of HG-LAFM. AFP staining was observed in a subset of cases (A). HG-LAFM frequently showed membranous and cytoplasmic staining for GPC-3 (B) and nuclear staining for SALL-4 (C). Neuroendocrine markers were positive in most cases (D, synaptophysin staining). Some tumors were positive for CDX-2 (E) and p53 (F).

GPC-3 and SALL-4, 2 sensitive markers of AFP-producing stomach cancer,[29,31,32] are often expressed in HG-LAFMs. The lung and stomach are both developed from the foregut, and AFP-producing stomach cancer and HG-LAFM (which might also produce AFP) might be regarded as showing similar oncofetal retrograde differentiation in terms of its morphology and immunoprofile. Intestinal marker CDX-2 expression, identified in 35% of our HG-LAFMs, might further suggest a close link between fetal lung–like histology in lung cancer and

TABLE 4. Molecular Characteristics of 17 High-grade Lung Adenocarcinomas With Fetal Lung–like Morphology

Case	*EGFR* Mutation	*KRAS* Mutation
1	WT	WT
2	L858R	WT
3	WT	WT
4	WT	WT
5	WT	WT
6	WT	Codon 12 or 13
7	WT	WT
8	WT	WT
9	WT	WT
10	WT	NA
11	WT	NA
12	WT	NA
13	WT	NA
14	NA	NA
15	NA	NA
16	NA	NA
17	WT	NA

NA indicates data not available; WT, wild type.

"primitive gut" differentiation in stomach cancer, because AFP-producing stomach cancers are usually of intestinal type and are positive for CDX-2.[33,34]

Results of molecular analysis suggest that HG-LAFM is not genetically homogenous. One case (7% of 14 cases tested) showed *EGFR* mutation. Another (11% of 9 cases tested) harbored *KRAS* mutation. However, it is notable that 78% of the 9 cases tested were of wild type for both *EGFR* and *KRAS*. Given the high frequency of *EGFR* and *KRAS* mutations (46% to 64% and 13%, respectively) in lung adenocarcinoma in the Japanese population,[35–37] this low rate might be worth investigation. The majority of HG-LAFMs (65%) showed positive p53 immunostaining. The rate of positivity in HG-LAFMs seems higher than that in lung adenocarcinoma in general (44% to 50%).[38,39]

In conclusion, HG-LAFM is associated with several characteristic clinicopathologic features such as male predominance, heavy smoking exposure, overrepresented coexistence with hepatoid, clear-cell, and high-grade neuroendocrine histology, and frequent immunoreactivity to neuroendocrine and oncofetal markers. Confirming the results in the original report[8] and providing additional morphologic and immunophenotypic characterization, our data indicate that HG-LAFMs might form a coherent subgroup of lung adenocarcinomas. However, the uniformly focal nature of fetal lung–like elements, widely diverse coexisting non–fetal lung–like histology, and inhomogenous molecular profiles make us hesitate to conclude that HG-LAFM truly constitutes a specific entity that is worthy of a separate entry in tumor classification. We believe that HG-LAFM is best considered for the time being as a recognizable morphologic pattern showing characteristic association with several clinicopathologic parameters. This treatment contrasts sharply with low-grade adenocarcinoma of fetal lung type, a distinct variant having homogenous fetal lung–like histology and specific genetic alteration. These 2 diseases should be confused neither in diagnostic reports nor in tumor classification. The morphologic and immunohistochemical similarity between HG-LAFM and AFP-producing stomach cancer is striking. This intriguing resemblance might open a new perspective to our understanding of HG-LAFM.

REFERENCES

1. Boyle P, Levin B. *World Cancer Report 2008*. Lyon: IARC Press, International Agency for Research on Cancer; 2008.
2. Travis WD, et al. World Health Organization, International Agency for Research on Cancer. *Pathology and Genetics of Tumours of the Lung, Pleura, Thymus, and Heart*. Lyon: IARC Press; 2004.
3. Kradin RL, Young RH, Dickersin GR, et al. Pulmonary blastoma with argyrophil cells and lacking sarcomatous features (Pulmonary endodermal tumor resembling fetal lung). *Am J Surg Pathol*. 1982;6:165–172.
4. Nakatani Y, Dickersin GR, Mark EJ. Pulmonary endodermal tumor resembling fetal lung: a clinicopathologic study of five cases with immunohistochemical and ultrastructural characterization. *Hum Pathol*. 1990;21:1097–1107.
5. Koss MN, Hochholzer L, O'Leary T. Pulmonary blastomas. *Cancer*. 1991;67:2368–2381.
6. Mardini G, Pai U, Chavez AM, et al. Endobronchial adenocarcinoma with endometrioid features and prominent neuroendocrine differentiation. A variant of fetal adenocarcinoma. *Cancer*. 1994;73:1383–1389.
7. Kodama T, Shimosato Y, Watanabe S, et al. Six cases of well-differentiated adenocarcinoma simulating fetal lung tubules in pseudoglandular stage. Comparison with pulmonary blastoma. *Am J Surg Pathol*. 1984;8:735–744.
8. Nakatani Y, Kitamura H, Inayama Y, et al. Pulmonary adenocarcinomas of the fetal lung type: a clinicopathologic study indicating differences in histology, epidemiology, and natural history of low-grade and high-grade forms. *Am J Surg Pathol*. 1998;22:399–411.
9. Nakatani Y, Miyagi Y, Takemura T, et al. Aberrant nuclear/cytoplasmic localization and gene mutation of beta-catenin in classic pulmonary blastoma - β-catenin immunostaining is useful for distinguishing between classic pulmonary blastoma and a blastomatoid variant of carcinosarcoma. *Am J Surg Pathol*. 2004;28:921–927.
10. Sekine S, Shibata T, Matsuno Y, et al. β-catenin mutations in pulmonary blastomas: association with morule formation. *J Pathol*. 2003;200:214–221.
11. Nakatani Y, Masudo K, Miyagi Y, et al. Aberrant nuclear localization and gene mutation of beta-catenin in low-grade adenocarcinoma of fetal lung type: up-regulation of the Wnt signaling pathway may be a common denominator for the development of tumors that form morules. *Mod Pathol*. 2002;15:617–624.
12. Sobin LH. Union internationale contre le cancer. *TNM Classification of Malignant Tumours*. Oxford: Wiley-Blackwell; 2009.
13. Travis WD, Brambilla E, Noguchi M, et al. International Association for the Study of Lung Cancer/American Thoracic Society/European Respiratory Society: international multidisciplinary classification of lung adenocarcinoma: executive summary. *Proc Am Thorac Soc*. 2011;8:381–385.
14. Arnould L, Drouot F, Fargeot P, et al. Hepatoid adenocarcinoma of the lung: report of a case of an unusual α-fetoprotein-producing lung tumor. *Am J Surg Pathol*. 1997;21:1113–1118.
15. Hayashi Y, Takanashi Y, Ohsawa H, et al. Hepatoid adenocarcinoma in the lung. *Lung Cancer*. 2002;38:211–214.
16. Ishikura H, Kanda M, Ito M, et al. Hepatoid adenocarcinoma: a distinctive histological subtype of alpha-fetoprotein-producing lung carcinoma. *Virchows Arch A Pathol Anat Histopathol*. 1990;417:73–80.
17. Kishimoto T, Yano T, Hiroshima K, et al. A case of α-fetoprotein-producing pulmonary carcinoma with restricted expression of